Petrology and geochemistry of D'Orbigny, geochemistry of Sahara 99555, and the origin of angrites

David W. Mittlefehldt[1], Marvin Killgore[2] and Michael T. Lee[3]

[1]mail code SN2, NASA/Johnson Space Center, Houston, TX 77058, USA

[2]Southwest Meteorite Lab, 202 South Clark St., Payson, AZ 85541, USA

[3]Hernandez Engineering Inc., 17625 El Camino Real, Houston TX 77058, USA

corresponding author's e-mail: david.w.mittlefehldt1@jsc.nasa.gov

Abstract—We have done detailed petrologic study of the angrite, D'Orbigny, and geochemical study of it and Sahara 99555. D'Orbigny is an igneous-textured rock composed of Ca-rich olivine, Al-Ti-diopside-hedenbergite, subcalcic kirschsteinite, two generations of hercynitic spinel and anorthite, with the mesostasis phases ulvöspinel, Ca-phosphate, a silico-phosphate phase and Fe-sulfide. We report an unknown Fe-Ca-Al-Ti-silicate phase in the mesostasis not previously found in angrites. One hercynitic spinel is a large, rounded homogeneous grain of a different composition than the euhedral and zoned grains. We believe the former is a xenocryst, the first such described from angrites. The mafic phases are highly zoned; mg# of cores for olivine are ~64, and for clinopyroxene ~58, and both are zoned to Mg-free rims. The Ca content of olivine increases with decreasing mg#, until olivine with ~20 mole% Ca is overgrown by subcalcic kirschsteinite with Ca ~30-35 mole%. Detailed zoning sequences in olivine-subcalcic kirschsteinite and clinopyroxene show slight compositional reversals. There is no mineralogic control that can explain these reversals, and we believe they were likely caused by local additions of more primitive melt during crystallization of D'Orbigny.

D'Orbigny is the most ferroan angrite with a bulk rock mg# of 32. Compositionally, it is virtually identical to Sahara 99555; the first set of compositionally identical angrites. Comparison with the other angrites shows that there is no simple petrogenetic sequence, partial melting with or without fractional crystallization, that can explain the angrite suite. Angra dos Reis remains a very anomalous angrite.

Angrites show no evidence for the brecciation, shock, or impact or thermal metamorphism that affected the HED suite and ordinary chondrites. This suggests the angrite parent body may have followed a fundamentally different evolutionary path than did these other parent bodies.

INTRODUCTION

Angrites form an enigmatic group of mafic igneous rocks that were formed on an asteroidal parent body very early in solar system history (*e.g.* Mittlefehldt *et al.*, 1998). They are characterized by Al-Ti-diopside-hedenbergite, Ca-rich olivine, kirschsteinite, anorthite and aluminous, Fe-rich spinels. Because they are rare, we have only a rudimentary understanding of the origin of the angrites. Thus, study of new angrites provides us with significant new information on the igneous processes that occurred on asteroids in the immediately post-natal solar system.

The first "comprehensive" study of angrites was done by Mittlefehldt and Lindstrom (1990), who did geochemical study of all three angrites known at that time. They showed that Lewis Cliff 86010 and Lewis Cliff 87051 were plausibly connected via olivine control, and that Angra dos Reis was compositionally distinct. Further, they suggested that angrites were formed by partial melting of carbonaceous chondrite-like source regions in which olivine and aluminous spinel were residual phases. Later, a fourth angrite, Asuka 881371 was recovered in Antarctica (Yanai, 1994), and showed petrologic and geochemical similarities particularly with LEW 87051 (Mikouchi *et al.*, 1996).

Recently, two new angrites have been found. Sahara 99555 is a 2.7 kg angrite from North Africa, and D'Orbigny is a 16.6 kg angrite from Argentina. Sahara 99555 is an igneous textured rock with mineralogical and petrographic similarities to the groundmass of A-881371 (Mikouchi *et al.*, 2000a,b). Preliminary petrologic descriptions show that D'Orbigny is a complex rock composed of two dense, crystalline fractions separated by a more porous fraction, and that it contains glass (Kurat *et al.*, 2001a,b; Varela *et al.*, 2001). The dense crystalline fraction is an igneous textured rock showing mineralogic and petrologic similarities to both A-

2

881371 and Sahara 99555 (Kurat *et al.*, 2001a; Mikouchi and McKay, 2001; Mittlefehldt *et al.*, 2001). The advent of two new, and large, angrites indicates that time is ripe to update the database on these rare meteorites, and reconsider the genesis of the group.

Here we report our completed petrologic and geochemical study of bulk samples of the compact portion of D'Orbigny. We have also done a comparative geochemical study of a bulk sample of Sahara 99555.

SAMPLES AND ANALYTICAL METHODS

We obtained a small chip of D'Orbigny from the finder for characterization. Several serial polished thin sections were made from this chip for petrographic observation and electron microprobe analysis (EMPA). From the remaining material, several small fragments were used to do instrumental neutron activation analysis (INAA) and fused-bead electron microprobe analysis (FB-EMPA) for major, minor and trace element characterization.

We did EMPA using the Cameca SX100 electron microprobe at NASA Johnson Space Center, and the Cameca SX50 electron microprobe at the University of Oklahoma. Analytical conditions for the SX100 probe were 20 kV, 40 nA for mafic silicates and oxides, and 15 kV 20 nA for plagioclase. Analytical conditions for the SX50 probe were 20 kV, 20 nA with a 2 μm beam for mafic silicates, oxides and plagioclase. Representative and average mineral analyses are given in Tables 1-4. We also did BSE and elemental mapping at JSC using 20 kV and 40 nA conditions.

We prepared two samples for geochemical analysis from the ~300 mg of chips used for this purpose. D'Orbigny is a find, and there is some rusting of the accessory sulfides in the

sample. From the chips, we handpicked those that appeared to be the least affected by the terrestrial environment. These chips, massing ~200 mg, were ground and homogenized, a ~56 mg split taken for INAA, and a ~25 mg split was used for major element analysis. This latter split of the homogenized powder was fused into a glass bead in an Ar atmosphere and analyzed for major elements via EMPA on the JSC SX100 probe. Analytical conditions were 15 kV, 15 nA with the beam rastered over a 10 x 10 μm area. The major element data are presented in Table 5.

INAA was done using standard JSC procedures (Mittlefehldt, 1994) in two irradiations. The results of the first INAA on D'Orbigny showed slightly higher than expected K, which we suspected might indicate terrestrial contamination. From the remaining chips of D'Orbigny, we removed potential terrestrial alteration material from the surfaces and handpicked the cleanest chips. These were further cleaned in ultra-pure water in an ultrasonic bath, dried and the entire sample was ground and used in the second irradiation. We also analyzed a small split of homogenized powder of Sahara 99555 prepared in L. Nyquist's clean laboratory. The exterior surface of this latter sample was mildly leached in 2N HCl prior to grinding. About 522 mg of Sahara 99555 was ground, homogenized and a 29 mg split was used for INAA. The results of our INAA on the angrites are given in Table 6. An average of our analyses of USGS standard sample BHVO-1 is also given, along with the recommended values.

PETROGRAPHY AND MINERAL CHEMISTRY

General

Our sample of D'Orbigny is an unshocked, unmetamorphosed, vesicular rock consisting of Al-Ti-diopside-hedenbergite (formerly called fassaite), Ca-rich olivine, subcalcic

4

kirschsteinite, anorthite, hercynitic spinel, ulvöspinel, Fe-sulfide, Ca-phosphate, a silico-phosphate phase, and an Fe-Ca-Al-Ti-silicate not previously reported from angrites. The overall texture is subophitic, with areas of graphic intergrowth of olivine+subcalcic kirschsteinite and anorthite (Fig. 1a). The Al-Ti-diopside-hedenbergite grains are up to ~3 mm long, generally subhedral with strong optical zoning. Anorthite grains are up to ~1 mm long, euhedral to subhedral, and often skeletal. Olivine grains are also up to ~1 mm long, euhedral to subhedral, and optically zoned. Hercynitic spinel occurs as ~50 μm euhedral grains enclosed in pyroxene and anorthite, but one of our thin sections also contains one ~0.8 mm rounded grain (Fig. 1b). Hercynitic spinel is surrounded by symplectic reaction boundaries. Ulvöspinel, Fe-sulfide, Ca-phosphate, silico-phosphate and Fe-Ca-Al-Ti-silicate occur in the mesostasis. Ulvöspinel grains are typically skeletal and roughly 100 μm in size. The silico-phosphate grains are euhedral to anhedral, about 10-20 μm in hexagonal cross section and ~100 μm in length. Groups of them are often poikilitically enclosed in clinopyroxene grain rims. The Fe-Ca-Al-Ti-silicate occurs as anhedral to subhedral grains ~50 μm in size. Iron sulfide occurs as irregular patches ~50-100 μm in size composed of numerous small, rounded grains.

Olivine and Subcalcic Kirschsteinite

Olivine is strongly zoned, and Ca-rich. Representative average olivine and subcalcic kirschsteinite compositions are given in Table 1. Olivine cores are homogeneous in composition; the most magnesian cores have molar 100*MgO/(MgO+FeO) (mg#) ~64, ~1.3 mole% Ca (100*Ca/(Ca+Mg+Fe)) (Fig. 2, 3) and contain 0.0008-0.0010 atoms per formula unit Cr. In general, olivine grains are zoned to about mg# 9 with Ca steadily increasing to about 20 mole%. These inner euhedral margins are overgrown by a band of subcalcic kirschsteinite (Fig. 4) with mg# 9 and 30-35 mole% Ca at the contact with olivine (Fig. 3). The subcalcic

kirschsteinite is zoned to mg# ~0 with 33-35 mole% Ca. Olivine again appears in the margins of the composite grains at ~mg# 6-5 and ~17-20 mole% Ca, where it is intergrown with the subcalcic kirschsteinite. This complex intergrowth persists to the edge of the grains at mg# 0.

In detail, the zoning sequence can be more complex (Fig. 4, 5). At the edge of the homogeneous olivine cores, the zoning sequence (first bright band in Fig. 4 BSE image) begins with a decrease in mg# coupled with an abrupt increase in Ca (Fig. 5). The mg# decreases to ~19, while Ca increases to ~ 10 mole % over a distance of ~24 μm in this grain. (Because we don't know whether the plane of the section is normal to the zoning bands, the distances cited are maxima.) In this zone, Cr decreases from the homogeneous core content down to the detection limit (about 0.0001-0.0002 apfu) over a distance as short as 10-15 μm. There is then a short reversal in zoning in which the mg# rises and the Ca content decreases slightly, while Cr remains essentially below detection, followed by a return to normal zoning with mg# decreasing to ~10 and the Ca content reaching ~18 mole%. The first bright band contains numerous dark spots (in BSE) of roughly μm size, which are not present elsewhere in the zoning profile (Fig. 4). These are rich in Ca, and Fe- and Mg-free (Ca-phosphate?). The olivine is overgrown by a band of zoned subcalcic kirschsteinite with mg# decreasing from ~9 to 5, while Ca remains relatively constant at ~35 mole%. Outside the subcalcic kirschsteinite zone is a zone of mixed olivine and subcalcic kirschsteinite (Fig. 4) where mg# steadily decreases to ~0 while the Ca contents of olivine and subcalcic kirschsteinite remain relatively constant (Fig. 5).

Al-Ti-Diopside-Hedenbergite

The clinopyroxene is Al-Ti-diopside-hedenbergite which varies in mg# from ~58 to 0 with >50 mole% Ca (Fig. 2). Representative average clinopyroxene compositions are given in

Table 2. The Ca and Ti contents show systematic variation with Mg (Fig. 6). At high Mg

(~0.55-0.20 apfu), the Ca content rapidly increases from ~0.94 to ~0.98 apfu, and thereafter

remains relatively constant while the Mg content decreases to 0. Likewise, the Ti content

increases while Mg decreases down to about 0.02 apfu. Titanium slightly decreases with a

further slight decrease in Mg, but reaches a relatively constant, though scattered, content of

~0.10 apfu through the remainder of the compositional sequence. Note that there are some

clinopyroxene grains with Ti contents distinct from the trend established by the majority (Fig. 6).

The Cr content of clinopyroxene steeply decreases with Mg content, and reaches the detection

limit when Mg is ~ 0.30 apfu (Fig. 6). Because Al is involved in coupled substitutions in

clinopyroxene with Ti and Cr, we show the Al-2*Ti-Cr (modified Al) content, effectively the

$R^{2+}Al_2SiO_6$ component, *vs.* Mg in Figure 6. This modified Al content is relatively constant for

Mg of 0.55 to ~0.15 apfu, and then gradually decreases with decreasing Mg. Some grains at

high Mg have unusually high modified Al. There are some grains with distinctly low modified

Al; these are the same grains with low Ti contents.

Zoning in clinopyroxene is illustrated in Figure 7. A 335 μm profile, taken from the

grain center to the rim shows slight decrease in mg# from ~58 to 53 over 170 μm, followed by

sharp decrease to ~0 at the rim. In detail, there are two breaks in mg# at ~110 and ~160 μm

where mg# slightly increased (Fig. 7c). The Cr content sharply decreases from the center out,

with two slight reversals at ~60 and 150 μm. Titanium is homogeneous in the central region, and

there are two offsets in the Ti profile at ~160 and 230 μm; the former coincides with the second

break in the mg# profile. Both Ti and Al-2*Ti-Cr show sharp variations in the outer ~100 μm.

These are not correlated, however, the spike in the Ti profile immediately precedes a spike in the

Al-2*Ti-Cr content, and these correlate with a sharp increase in the Ca content.

Spinels

There are three distinct spinel phases: (i) a single large, rounded hercynitic spinel (Fig. 1b), (ii) smaller hercynitic spinel enclosed in plagioclase and clinopyroxene, and (iii) ulvöspinel in the mesostasis. The core of the large hercynitic spinel (Fig. 1b) is homogeneous over a distance of at least 300 μm, with the composition $Hc_{32.5}Sp_{55.5}Cm_{9.0}Uv_{0.5}Mt_{2.5}$ (Table 3, Fig. 8). The smaller hercynitic spinel grains are typically enclosed in clinopyroxene and plagioclase, and show ghost euhedral outlines - the grains now consist of variably rounded cores with symplectic borders that show the original euhedral outlines of the grains (Fig. 9). The small grains are distinct in composition from the large, rounded grain (Fig. 8). They contain a lower spinel component yet higher chromite component, and are zoned showing increasing hercynite with decreasing spinel and chromite (Table 3, Fig. 8) over distances of 20-30 μm. Both the large and small hercynitic spinels have symplectic reaction rims containing spinels that are richer in Fe^{2+}, Fe^{3+}, Ti and sometimes Cr, and poorer in Al and Mg. The two grains shown in Fig. 9 have semi-continuous borders composed of μm-sized Cr-rich spinel grains. The mesostasis ulvöspinel grains are typically euhedral skeletal grains about 100 μm across, with relatively uniform compositions of $Hc_{4.5-7.5}Sp_{0.1-0.4}Cm_{0.0}Uv_{71.1-77.4}Mt_{17.6-21.4}$ (Table 3).

Mesostasis Phases and Plagioclase

Silico-phosphate is a poorly characterized phase found in some angrites (Kaneda *et al.*, 2001; Mikouchi *et al.*, 2000a; Mittlefehldt *et al.*, 2001; Prinz and Weisberg, 1995; Warren and Davis, 1995). In D'Orbigny, silico-phosphate is relatively homogeneous in composition, although we did find one grain with a distinctly different composition (Table 4). We have not done extensive study of this phase, however.

We have discovered an unidentified phase in the mesostasis not previously been reported from angrites. This phase is homogeneous in composition (Table 4) and has a cation/Si ratio of ~2.65.

Plagioclase is ~An_{100}, with 0.5-0.8 wt% FeO and 0.1-0.3 wt% MgO (Table 4).

GEOCHEMISTRY

The major element composition and CIPW normative mineralogy of D'Orbigny and other angrites are given in Table 5, and select major, minor and trace element contents of D'Orbigny and Sahara 99555 are given in Table 6. Like other angrites, D'Orbigny is highly depleted in Na, with a bulk rock Na_2O content of 0.017 wt%, and has Ca/Al greater than the CI ratio. All angrites are critically silica-under saturated, with normative nepheline and Ca_2SiO_4 (Cs). The FeO content is slightly higher, while the MgO content is slightly lower in D'Orbigny than for any other angrite, giving it the lowest mg# among angrites. D'Orbigny has a low Cr_2O_3 content, 0.042 wt%, roughly a third the content of the next lower angrite, LEW 86010.

Our INAA data on D'Orbigny and Sahara 99555 (Table 6) show that these two meteorites have very similar compositions. They both have the unusually low Cr contents and slightly high FeO. They have similar Co contents, which are higher than found for other angrites, except A-881371 (Mittlefehldt and Lindstrom, 1990; Warren et al., 1995 – Warren et al. give a preliminary Co content for A-881371 of 51 $\mu g/g$). The rare earth elements (REE), Hf, Ta and Th in D'Orbigny and Sahara 99555 are also nearly identical; the REE in particular show a clear distinction between D'Orbigny and Sahara 99555 on the one hand, and all other angrites on the other (Fig. 10). This is the first case in which two angrites are essentially identical in composition. Although absolute abundances of incompatible lithophile elements distinguish all

angrites from one another (excluding D'Orbigny and Sahara 99555), the Sm normalized patterns

for all of them, excluding Angra dos Reis, are very similar (Fig. 11).

DISCUSSION

Among meteorite classes, a large number of differentiated parent bodies are represented.

Most of these are represented only by deep-seated igneous materials - the various magmatic iron

meteorites and pallasites (*e.g.* see Mittlefehldt *et al.*, 1998). There are relatively few crustal

igneous materials, *i.e.* basalts, in our meteorite collections. Rare basaltic/gabbroic segregations

and clasts are present in the acapulcoite-lodranite suite, in some IAB irons and in some IIE irons

(*e.g.*, Ikeda *et al.*, 1997; McCoy *et al.*, 1997; Takeda *et al.*, 2000). Because of the unusual

textural settings of these segregations and clasts, it is difficult to completely understand their

genesis. There are two igneous meteorite groups containing a large fraction of basaltic material;

the large howardite, eucrite diogenite (HED) suite and the small angrite group. The HED suite is

largely composed of breccias in which many of the components have undergone thermal

metamorphism (*e.g.* see Mittlefehldt *et al.*, 1998). Hence, the magmatic processes responsible

for the formation of the HED parent body crust have been partially obscured. The angrites, in

contrast, have suffered less post-crystallization modification, and thus are a truer record of

asteroidal igneous processes. Unhappily, the angrite group is small, six members so far, so the

range of materials available for study is severely limited.

Here, we will discuss first the detailed petrology of D'Orbigny, compare it to the other

angrites, and discuss the composition of D'Orbigny and Sahara 99555. We will fold this

information into the broader picture of angrite petrogenesis, and finally, compare and contrast

the evolution of the angrite parent body with that of the HED meteorite suite.

Petrology and Crystallization of D'Orbigny

The most unusual aspect of our thin sections of D'Orbigny is the large, rounded spinel grain that occurs in one of them (Fig. 1b). A similar textural setting for spinel has not been reported for other angrites. This spinel grain is homogeneous over a scale of at least 300 μm, while the smaller euhedral grains are zoned on scales of a few tens of μm (Figs. 8, 9). The large spinel is also distinct in composition, with the unusual combination of being more magnesian, yet poorer in chrome (Fig. 8). The combined textural and compositional characteristics suggest that the large spinel is xenocrystic material in this angrite, like the proposed origin for the magnesian, chrome-rich coarse olivine grains in LEW 87051, Asuka 881371 and other samples of D'Orbigny (*e.g.* Kurat *et al.*, 2001b; Mikouchi and McKay, 2001; Mikouchi *et al.*, 1996).

Most angrites contain coarse magnesian, chrome-rich olivine grains that are believed to be xenocrystic in origin (*e.g.* see Mikouchi *et al.*, 1996). Our thin sections of D'Orbigny do not contain them. The smaller, euhedral olivine grains contain cores that are homogeneous in mg#, and minor element content (Fig. 5), and similar in composition to those reported from Sahara 99555 (Mikouchi *et al.*, 2000a,b). There is a sharp boundary between the homogeneous core and strongly zoned rim (Fig. 4). Based on our preliminary data, we suggested that this might indicate a two stage cooling history (Mittlefehldt *et al.*, 2001). However, we now believe that this indicates a stage in the crystallization history when the second major mafic phase, clinopyroxene, began crystallizing. Support for this position comes from the detailed zoning profile (Fig. 5). The zoned rim is marked by a sharp drop in Cr_2O_3 in the olivine, along with a decrease in mg#. The most magnesian olivine cores contain about 0.043 wt% Cr_2O_3 (Table 1), essentially the same as the bulk rock (Table 5). Hence, assuming these cores are phenocrysts, the olivine/melt Cr partition coefficient is ~1, which is consistent with experimental studies

(Jones, 1995). Crystallization of olivine will therefore not change the melt Cr_2O_3 content appreciably, consistent with the constant concentration in the core. In contrast, the most magnesian clinopyroxene contains about 0.54 wt % Cr_2O_3, yielding an effective clinopyroxene/melt partition coefficient of ~10, and the Cr content of clinopyroxene decreases sharply with mg# (Figs. 6, 7). Because of this, we now believe that the initiation of zoning in olivine reflects the onset of clinopyroxene crystallization, and not a change in cooling environment.

The details of the zoning profile in olivine show slight reverse zoning in mg# from ~18 to 20, and in Ca content from ~9.7 to 7.0 mole% (Fig. 5), and this is correlated with a mottled zone in the first bright band (Fig. 4). This reversal, and the texture showing scalloped borders for the reversal (Fig. 4), suggest the melt composition became slightly more magnesian and with a higher Si activity (which will cause a decrease in olivine Ca content) at this point. We do not find a good mineralogical explanation for this reversal. One phase that could cause an increase in melt Mg/Fe and Si activity is ulvöspinel. However, this phase occurs as a late phase in the mesostasis, and the textures indicate that it did not appear early enough in the crystallization sequence to explain the reverse zoning. In addition, this would not explain why the zoning returns to normal after a short span of crystallization. Neither is the reverse zoning caused by crystallization of the hercynitic spinels. The cores of these spinels have molar Mg/Fe ratios of ~1, compared to the bulk rock ratio of ~0.5. Hence, crystallization of hercynitic spinel will further deplete the melt in Mg and not cause reverse zoning in olivine. A third possibility is that it represents an influx of more primitive melt causing back-reaction of the olivine grain surfaces. Detailed ion microprobe studies across the zone may shed light on this. D'Orbigny contains glasses with compositions like the bulk rock composition (Varela *et al.*, 2001; see Table 5) that

12

must have entered the stone after crystallization. The zoning profile in clinopyroxene also shows

reversals in mg# and Cr, and offsets in Ti (Fig. 7) which may indicate ingress of distinct melts.

The Cr reversals in particular suggest this, as an increase in Cr content in the melt phase is

unlikely to be caused by crystallization of other phases. Finally, the small euhedral spinels often

contain Cr-rich rims, even when enclosed in anorthite (Fig. 9), which suggests that more Cr-rich

melts may have been responsible for the reaction that formed the rims. This petrographic

evidence suggests that multiple magma batches may have been locally present during

crystallization of D'Orbigny. Whether this represents additions of new magma from the parent

body interior, or simple stirring of the crystallizing, heterogeneous magma during flow, cannot

be determined at present.

The zoned olivine contains overgrowths of zoned subcalcic kirschsteinite on euhedral

olivine outlines (Fig. 4). There is a distinct gap in olivine compositions; we find no olivine

compositions between mg# ~9 and ~6-5 (Figs. 2, 3). The texture suggests that the subcalcic

kirschsteinite overgrowths are magmatic. Outside the euhedral subcalcic kirschsteinite margin is

a zone of mixed subcalcic kirschsteinite and olivine, indicating that towards the end of

crystallization, olivine and subcalcic kirschsteinite co-crystallized.

Clinopyroxene also contains relatively homogeneous cores (in mg# and Ti) and zoned

rims, but the cores are not as uniform as those in olivine (Fig 7). Note that the core region of the

clinopyroxene grain shows a marked decrease in Cr content with only a slight change in mg#.

This is consistent with our contention that clinopyroxene crystallization initiates zoning in the

olivine. The core region also shows slight decreases in Al-2*Ti-Cr, indicating that the non-

quadrilateral component $R^{2+}Al_2SiO_6$ in clinopyroxene initially decreases. The zoning profile in

the rim region shows a substantial decrease in mg# and Al-2*Ti-Cr, and a substantial increase in

Ti and Ca (Fig. 7). Both Ti and Al-2*Ti-Cr show small scale "spikes" that indicate abrupt increases in the non-quadrilateral components. Note that we have done only one detailed profile across a clinopyroxene grain, and if sector zoning is present, than this profile may not by representative of all zoning variations.

Plagioclase was likely a near-liquidus phase as it commonly forms graphic intergrowths with olivine, indicating co-crystallization. There is much less intergrowth between plagioclase and clinopyroxene. Because of the lack of Na and K in D'Orbigny, plagioclase compositions cannot be used to examine the crystallization history of this phase. Although there is variation in the MgO and FeO contents of plagioclase, we have not found systematic zoning in these minor components. In part this is due to the skeletal and intergrown nature of many of the grains, making growth fronts difficult to identify with certainty.

The euhedral hercynitic spinels are commonly included within clinopyroxene and plagioclase grains, but don't extend into the mesostasis (Fig. 9). In addition, they typically show reaction boundaries of variable thickness. This suggests that hercynitic spinel crystallization began early, and then became unstable in the changing melt. Based on our preliminary results, we suggested that spinel was a liquidus phase along with olivine in part because of the presence of the large hercynitic spinel grain (Mittlefehldt *et al.*, 2001). However, we now consider this spinel to be xenocrystic, and we have not observed a textural association between the magnesian olivine cores and the small euhedral hercynitic spinel. Thus we cannot precisely determine when this spinel appeared in the crystallization sequence. Figure 12 shows the crystallization sequence we infer for D'Orbigny.

The extreme compositional zonation of minerals and the presence of late-stage, trace phases in the mesostasis (Ca-phosphate, silico-phosphate, unknown Fe-Ca-Al-Ti-silicate) in D'Orbigny indicate that this rock underwent rapid, complete crystallization; D'Orbigny represents a melt composition. This is also suggested by the observed variations in trace elements in clinopyroxene and olivine (Floss *et al.*, 2001). Note however, that our observations suggesting that more than one melt may be involved in the genesis of D'Orbigny, if true, might indicate that this is a hybrid composition, not a single melt composition.

Comparison of D'Orbigny with Other Angrites

D'Orbigny is texturally most similar to Sahara 99555, or the groundmass fractions of Asuka 881371 and Lewis Cliff 87051 (Mikouchi and McKay, 2001; Mittlefehldt *et al.*, 2001). Mikouchi *et al.* (2000a,b) presented a brief description of Sahara 99555. Sahara 99555 shares many similarities with D'Orbigny – the vesicular nature of the stone, the igneous texture with common olivine-anorthite graphic intergrowths, and the compositions of the minerals are very similar. Mikouchi and McKay (2001) further show that mineral compositions in Sahara 99555 and D'Orbigny almost completely overlap. Olivine cores in Sahara 99555 have mg# of ~63 and contain ~0.8 wt% CaO (Mikouchi *et al.*, 2000a,b), essentially identical to D'Orbigny (this work; Mikouchi and McKay, 2001). Mikouchi and McKay (2001) find slightly more magnesian clinopyroxene cores than we do; their most magnesian clinopyroxene has an mg# of ~63, compared to ~58 in our thin sections. These are more magnesian than any reported for Sahara 99555 (mg# <50; Mikouchi *et al.*, 2000a,b).

Although there are greater textural similarities between D'Orbigny and Sahara 99555, mineral compositions of D'Orbigny more closely match those of the groundmass fraction of A-

881371. The most magnesian olivine phenocrysts, kirschsteinite and clinopyroxene of A-881371 (Mikouchi *et al.*, 1996) are only slightly more magnesian than the most magnesian mafic phases in D'Orbigny (Fig. 2). The cores of olivine phenocrysts in LEW 87051 have mg# ~80 (McKay *et al.*, 1995; Mikouchi *et al.*, 1996), substantially higher than those of D'Orbigny. Nevertheless, the most magnesian clinopyroxene and subcalcic kirschsteinite grains in LEW 87051 are very similar to those of D'Orbigny (Fig. 2). McKay *et al.* (1995) show (their Fig. 2) magnesian clinopyroxene grains with mg# slightly less than 60, and with TiO_2, Al_2O_3 and Cr_2O_3 contents within the ranges we find of D'Orbigny magnesian clinopyroxene grains (Table 2).

Our thin sections of D'Orbigny do not contain the xenocrystic, magnesian olivine found in A-881371 and LEW 87051, although other samples do (Kurat *et al.*, 2001b; Mikouchi and McKay, 2001). Mikouchi and McKay (2001) estimate that magnesian olivine xenocrysts make up roughly 1% of D'Orbigny, compared to ~10% of A-881371 and LEW 87051. They further point out that olivine xenocrysts have not been reported from Sahara 99555. In view of the heterogeneous nature of xenocryst distribution in D'Orbigny and its low abundance, it may well be that they also occur in Sahara 99555, which has not been extensively sampled. Deep-seated xenoliths and xenocrysts are common in terrestrial alkaline volcanic rocks and indicate that the magmas rose rapidly from depth without pause. Possibly, the xenocrysts in angrites may similarly indicate that the parent magmas rose rapidly, entraining pieces of country rock along the way. The vesicular nature of D'Orbigny and Sahara 99555 indicate that volatile species were present in the magmas, and these would promote rapid eruption on an asteroid-size parent body (*e.g.* see Wilson and Keil, 1997).

D'Orbigny is very different in texture, modal mineralogy and/or mineral composition from Angra dos Reis and LEW 86010. Angra dos Reis is an almost mono-mineralogic rock,

composed of >90% clinopyroxene, with an equilibrated texture, and plagioclase has not been found in thin section (Prinz *et al.*, 1977). LEW 86010 has a modal mineralogy similar to that of D'Orbigny (compare McKay *et al.*, 1988a; Mikouchi and McKay, 2001), but its texture is more equilibrated (McKay *et al.*, 1988a). Mineral compositions in Angra dos Reis and LEW 86010 are distinct from those of D'Orbigny. Comparing the most magnesian phases in each meteorite, clinopyroxenes are more magnesian, kirschsteinites are more magnesian and calcic, and olivines are more ferroan in the former two meteorites than in D'Orbigny (Fig. 2).

Geochemistry of D'Orbigny and Sahara 99555, and Angrite Petrogenesis

Mittlefehldt and Lindstrom (1990) pointed out that the three angrites known at that time had super-chondritic Ca/Al ratios, and were distinct from basaltic eucrites in that regard. Figure 13 shows CI-normalized Sm/Eu *vs.* Ca/Al for angrites compared to basaltic eucrites. Excluding Angra dos Reis, all angrites have $(Ca/Al)_{CI} \sim 1.5$ and $(Sm/Eu)_{CI} \sim 1.0$. In contrast, basaltic eucrites have $(Ca/Al)_{CI} \sim 1.0$ and $(Sm/Eu)_{CI} \sim 0.8\text{-}1.7$. Mittlefehldt and Lindstrom (1990) argued that the high Ca/Al ratio of angrites was not due to plagioclase fractionation because the $(Ca/Al)_{CI}$ ratio of anorthite (0.7) is too close to unity to efficiently fraction the Ca/Al of a melt, while the Sm/Eu ratio should be substantially fractionated by plagioclase. Figure 13 empirically demonstrates this. The basaltic eucrite suite has experienced plagioclase fractionation (*e.g.* see Mittlefehldt *et al.*, 1998; Stolper, 1977), yet shows little variation in Ca/Al but substantial variation in Sm/Eu. In contrast, all angrites, excluding Angra dos Reis, show a narrow range in Sm/Eu indicating that plagioclase fractionation was not a significant factor in angrite genesis.

Summarizing geochemical, petrologic and experimental results on angrites, Mittlefehldt and Lindstrom (1990) concluded that residual aluminous spinel in the source regions of angrites

was the most probable cause for the elevated Ca/Al in angrites. Experimental support for this was found by Jurewicz *et al.* (1993), who showed that partial melting of CM and CV chondrites under f_{O_2} conditions appropriate for angrite genesis did yield melts with Ca/Al ratios like those of angrites, and that aluminous spinel was a residual phase in all experiments. The addition of two new angrites, A-881371 (Warren *et al.*, 1995; Yanai, 1994) and D'Orbigny confirm that angrites (excluding Angra dos Reis) have uniform and elevated Ca/Al ratios consistent with buffering by aluminous spinel.

Mittlefehldt and Lindstrom (1990) suggested that the difference in major and trace element contents of LEW 86010 and LEW 87051 was consistent with simple olivine control, that is, with either gain or loss of olivine from a common magma. With additional angrites and more information on the older samples we can revisit this hypothesis. Figure 14 shows Sm *vs.* mg# and Sc *vs.* mg# for angrites. We have plotted A-881371 and LEW 87051 both as measured for bulk rocks (Mittlefehldt and Lindstrom, 1990; Warren *et al.*, 1995; Yanai, 1994), and using the estimated groundmass compositions (Prinz and Weisberg, 1995) with Sm and Sc estimated here assuming olivine xenocrysts are Sm- and Sc-free. Samarium and Sc are incompatible elements, so their concentrations should increase as melt mg# decreases due to fractional crystallization of olivine (schematically shown in Fig. 14, arrows labeled fc). In the angrite suite, we see the opposite trend; Sm and Sc decrease as mg# decreases for LEW 86010, LEW 87051 groundmass and D'Orbigny. Potentially, A-881371 groundmass could be related to either LEW 87051 groundmass or D'Orbigny by olivine removal from A-881371. Based on trace element variations in angrite clinopyroxenes, Floss *et al.* (2000) concluded that LEW 86010 crystallized from a distinctly different magma from the other angrites they studied.

Based on cosmochemical and phase equilibria arguments, and experimental studies, olivine is expected to be the major residual mafic silicate after partial melting in the angrite parent body (*e.g.*, Jurewicz *et al.*, 1993; Longhi 1999; McKay *et al.*, 1988; Mittlefehldt and Lindstrom, 1990). Partial melting in which olivine is the major residual phase will result in a trend of decreasing Sm and Sc with slightly increasing mg# (schematically shown in Fig. 14, arrows labeled pm). In the angrite suite, D'Orbigny cannot be related to LEW 86010, LEW 87051 and A-881371 by simple partial melting. However, LEW 86010, LEW 87051 and A-881371 could potentially represent a suite of increasing degree of partial melting, with LEW 86010 representing a melt derived by a smaller degree of melting than A-881371 (Fig. 14). However, mineral compositions show that this is not the case. LEW 86010 contains clinopyroxene cores with higher mg# than those in A-881371 (Fig. 2), and this is opposite what would be expected if LEW 86010 represented a smaller degree of melting. Hence, we conclude that there is not a simple partial melting-fractional crystallization scenario joining the angrites. This is distinctly different from what is observed for the HED suite (Stolper, 1977).

Longhi (1999) has discussed the petrogenesis of the angrites using phase equilibria in the CMAS+Fe system. The crystallization sequence in this system is complicated by shifting phase relations as mg# changes during fractional crystallization. However, Longhi (1999) showed that A-881371, LEW 86010 and LEW 87051 plot within the olivine+plagioclase field, indicating these two phases are liquidus phases, consistent with petrography and limited experimental work (McKay *et al.*, 1988a,b; 1991; Mikouchi *et al.*, 1996). Note that Longhi (1999) used the bulk A-881371 and LEW 87051 compositions, not the estimated groundmass compositions, which are closer to melt compositions. While spinel is not a liquidus phase in this case, Longhi (1999)

pointed out that addition of Cr and Ti to the system would likely expand the stability field of spinel.

A schematic phase diagram after Longhi (1999) relevant to angrite petrogenesis is shown in Fig. 12. We have added D'Orbigny and the A-881371 and LEW 87051 groundmass compositions, and our inferred crystallization path to the diagram. Like all other angrites except Angra dos Reis, D'Orbigny plots within the olivine+plagioclase phase field, and crystallization starts with these phases (arrow labeled 1). Hercynitic spinel may join the crystallization sequence during this part of the path, but the textural and phase relations are not clear. At 2, the crystallization sequence becomes olivine+plagioclase+clinopyroxene. If hercynitic spinel is not already a liquidus phase, it joins the crystallization sequence at about this point. The phase diagram suggests that at 3, the crystallizing assemblage becomes olivine+clinopyroxene+spinel, followed at 4 by olivine+clinopyroxene+spinel+kirschsteinite. The textures of D'Orbigny suggest rather that spinel reacts-out before 3 is reached, and that kirschsteinite temporarily replaces olivine in the crystallization sequence at 4.

Angra dos Reis – Odd Man Out

We have generally avoided discussing Angra dos Reis up to this point, for good reason. Based on modal mineralogy (*e.g.* see Mittlefehldt *et al.*, 1998) and bulk major and trace element composition (Figs. 10, 11, 13, 14), Angra dos Reis is anomalous compared to all other angrites. The irony of using it as the type example and namesake for the group is exquisite, and points out the dangers of defining meteorite groups based on too few examples. Nevertheless, Angra dos Reis is clearly closely related to the other angrites in oxygen-isotope composition and in its unusual mineralogy (see Mittlefehldt *et al.*, 1998). Mittlefehldt and Lindstrom (1990) suggested

20

that either Angra dos Reis was formed from a distinctly different source region on the angrite parent body, or on a separate parent body than LEW 86010 and LEW 87051. Longhi (1999) has also concluded that Angra dos Reis requires a different source region.

The three newest angrites A-881371, D'Orbigny and Sahara 99555 serve to amplify the anomalous character of Angra dos Reis relative to the group. Sioux County- and Sm-normalized incompatible refractory lithophile element patterns for all angrites except Angra dos Reis are very similar (Fig. 11), indicating a basic commonality in petrogenesis. Angra dos Reis shows extreme fractionations in R^{2+}, Al, Sc, La, Hf and U (Fig. 11) when compared to other angrites. Longhi (1999) suggested that the difference in major element composition, and hence crystallization paths, between Angra dos Reis and the other angrites might possibly explain at least a portion of the difference in REE contents between them. He suggested that Angra dos Reis was a cumulate containing trapped melt, and noted that clinopyroxene/melt partition coefficients relevant to Angra dos Reis genesis might be up to twice as large as for the other angrites. This would serve to reduce the disparity between Angra dos Reis and LEW 86010 REE contents (Fig. 10). However, based on experimental partitioning studies (Gaetani and Grove, 1995), one would expect the aluminous clinopyroxenes to also have a much higher Sc partitioning coefficient. Gaetani and Grove (1995) showed that Ce^{3+} and Yb^{3+} clinopyroxene/ melt partition coefficients increased with increasing clinopyroxene $CaAl_2SiO_6$ content, and that the smaller Yb^{3+} increased more than the larger Ce^{3+}. It is plausible then that partitioning of the smaller Sc^{3+} should also substantially increase in aluminous clinopyroxenes. The low Sc/Sm ratio for Angra dos Reis (Fig. 11, and see Mittlefehldt *et al.*, 1998, Fig. 52b) is then difficult to explain.

What's up with Angrites?

The angrites, as basalts formed very early in solar system history on an asteroid-sized body, share a basic formational history with the eucrites. However, there is a strong textural dichotomy between these two groups. Most eucrites have been thermally metamorphosed, most are breccias, and many show evidence for shock metamorphism (*e.g.* see Delaney *et al.*, 1983; Mittlefehldt *et al.*, 1998; Takeda and Graham, 1991). We now have six angrites, three of considerable size. The cosmic ray exposure ages of them are all different (Bischoff et al., 2000; Eugster et al., 1991; Kurat et al., 2001a; Lugmair and Marti, 1977; Weigel *et al.*, 1997)) indicating that multiple regions of the parent body surface were likely sampled. None of them are breccias, none show evidence for shock metamorphism, and with the exceptions of Angra dos Reis and LEW 86010, thermal metamorphism is not evident. In LEW 86010, thermal metamorphism has equilibrated the compositions of olivine and kirschsteinite, but not that of clinopyroxene (Mikouchi *et al.*, 1996). In contrast, most eucrites have had their pyroxene compositions substantially equilibrated by thermal metamorphism (Takeda and Graham, 1991). This difference in thermal and impact metamorphism plausibly indicates that there is some fundamental difference between the angrite and eucrite parent bodies.

Bogard (1995) has suggested that the large number of young, reset Ar-Ar ages among lunar samples and eucrites is due to the inner-solar-system-wide late heavy bombardment, and that the Ar-Ar ages will be reset only in large impacts, suggesting that these parent bodies were relatively large. The surface rocks of these parent bodies thus became extensively brecciated and shock-metamorphosed. If true, this might suggest that either the angrite parent body was small, or that it formed in a region of the solar system less affected by the late heavy bombardment. The latter seems unlikely as spacecraft observations show that solid surfaces in the inner solar system from Mercury to the moons of Jupiter have suffered extensive impact modification.

Chondrites are generally believed to be derived from smaller parent bodies, yet many of them are brecciated and have suffered impact metamorphism (Brearley and Jones, 1998). Bogard (1995) argued that the large number of very young ages (<1.5 Ga) for chondrites (mostly ordinary chondrites) is consistent with their being derived on small parent bodies that were susceptible to catastrophic disruption and age resetting. Only three of the angrites have had formation ages determined, but they are all among the oldest objects in the solar system, and there is no evidence for later disturbance in their ages (Lugmair and Galer, 1992; Lugmair and Marti, 1977; Nyquist *et al.*, 1994; Premo and Tatsumoto, 1995; Wasserburg *et al.*, 1977) or in their textures. Thus, angrites have followed an evolutionary history that appears fundamentally different from that of the smaller asteroids that coughed-up chondrites.

Regardless, either scenario for explaining the pristine nature of angrites (small body, special location) has implications for our understanding of the heat source that melted asteroids. Most models suggest that the mechanism that heated meteorite parent bodies was either heliocentric, or more efficacious on larger bodies (Wood and Pellas, 1991), and are therefore at odds with the angrites having formed either on a small parent body, or on one outside the range of the late-heavy bombardment. Thus, continued study of the angrites and comparison with eucrites may bring the mysterious early solar system heat source into sharper focus.

CONCLUSIONS

D'Orbigny is an unshocked, unmetamorphosed, vesicular igneous rock consisting of Al-Ti-diopside-hedenbergite, Ca-rich olivine, subcalcic kirschsteinite, anorthite, hercynitic spinel, ulvöspinel, Fe sulfide, Ca-phosphate, a silico-phosphate phase, and an Fe-Ca-Al-Ti-silicate not previously reported from angrites. The mafic silicates are extremely zoned, from mg# of 64 (olivine) and 58 (clinopyroxene) to essentially Mg-free rims. Details of zoning profiles in

composite olivine-subcalcic kirschsteinite grains and in clinopyroxene grains show that brief reversals in zoning occurred during crystallization. There appears to be no obvious mineralogic control that can explain these reversals, and we suggest that they were caused by additions of more primitive melt during the crystallization sequence. This could be either addition of new magma from the parent body interior, or stirring of a heterogeneous magma as it flows. Hence, although the textures and mineral compositions show that D'Orbigny represents a crystallized melt composition, this melt may have been a hybrid composition.

The trace and select major element compositions of D'Orbigny and Sahara 99555 are virtually identical; the first such case in the angrite suite. D'Orbigny is the most Fe-rich angrite, with a bulk rock mg# of 32. Like all angrites, D'Orbigny has a fractionated Ca/Al ratio, and all but Angra dos Reis have a chondritic Sm/Eu ratio. These indicate that plagioclase fractionation did not play a significant role in angrite genesis, and that fractionation of aluminous spinel did. There is no simple set of partial melting with or without fractional crystallization scenarios that can explain the bulk rock and mineral core compositions in the angrite suite. Angra dos Reis remains a very anomalous angrite, and there is no obvious, simple petrogenetic scheme that relates it to the others.

The angrites somehow missed the thermal metamorphism, brecciation and shock processes that affected the HED suite and ordinary chondrites. The reasons for this are obscure, but we believe this possibly bespeaks a fundamentally different history for the angrite parent body.

REFERENCES

Bischoff A., Clayton R.N., Markl G., Mayeda T.K., Palme H., Schultz L., Srinivasan G., Weber H.W., Weckwerth G. and Wolf D. (2000) Mineralogy, chemistry, noble gases, and oxygen- and magnesium-isotopic compositions of the angrite Sahara 99555 (abstract). *Meteoritics Planet. Sci.* **35,** A27.

Bogard D.D. (1995) Impact ages of meteorites: A synthesis. *Meteoritics* **30,** 244-268.

Brearley A.J. and Jones R.H. (1998) Chondritic meteorites. In *Planetary Materials* (ed. J.J. Papike), pp. 3-1 to 3-398. Reviews in Mineralogy, **36,** Min. Soc. Am., Washington, D.C., USA.

Crozaz G. and McKay G. (1990) Rare earth elements in Angra dos Reis and Lewis Cliff 86010, two meteorites with similar but distinct magma evolutions. *Earth Planet. Sci. Lett.* **97,** 369-381.

Delaney J.S., Takeda H., Prinz M., Nehru C.E. and Harlow G.E. (1983) The nomenclature of polymict basaltic achondrites. *Meteoritics* **18,** 103-111.

Eugster O., Michel Th. and Niedermann S. (1991) [244]Pu-Xe formation and gas retention age, exposure history, and terrestrial age of angrites LEW86010 and LEW87051: Comparison with Angra dos Reis. *Geochim. Cosmochim. Acta* **55,** 2957-2964.

Floss C., Crozaz G. and Mikouchi T. (2000) Sahara 99555: Trace-element compositions and relationship to Antarctic angrites (abstract). *Meteoritics Planet. Sci.* **35,** A53.

Floss C., Killgore M. and Crozaz G. (2001) Trace element compositions and petrogenesis of the D'Orbigny angrite (abstract). *Lunar Planet. Sci.* **32,** #1201.

Gaetani G.A. and Grove T.L. (1995) Partitioning of rare earth elements between clinopyroxene and silicate melt: Crystal-chemical controls. *Geochim. Cosmochim. Acta* **59,** 1951-1962.

Govindaraju K. (1994) 1994 compilation of working values and sample descriptions for 383 geostandards. *Geostandards Newslett.* **18,** *Sp. Issue,* 158 pp.

Ikeda Y., Ebihara M. and Prinz M. (1997) Petrology and chemistry of the Miles IIE iron. I: Description and petrology of twenty new silicate inclusions. *Proc NIPR Symp. Antarctic Meteorites* **10,** 143-173.

Jones J.H. (1995) Experimental trace element partitioning. . In *Rock Physics and Phase Relations. A Handbook of Physical Constants,* 73-104.

Jurewicz A..G., Mittlefehldt D.W. and Jones J.H. (1993) Experimental partial melting of the Allende (CV) and Murchison (CM) chondrites and the origin of asteroidal basalts. *Geochim. Cosmochim. Acta* **57,** 2123-2139.

Kurat G., Brandstätter F., Clayton R., Nazarov M.A., Palme H., Schultz L., Varela M.E., Wäsch E., Weber E. and Weckwerth G. (2001a) D'Orbigny: A new and unusual angrite (abstract). *Lunar Planet. Sci.* **32,** #1753.

Kurat G., Varela M.E., Brandstätter F., Wäsch E. and Nazarov M.A. (2001b) D'Orbigny: A new window into angrite genesis (abstract). *Lunar Planet. Sci.* **32,** #1737.

Longhi J. (1999) Phase equilibrium constraints on angrite petrogenesis. *Geochim. Cosmochim. Acta* **63,** 573-585.

Lugmair G.W. and Galer S.J.G. (1992) Age and isotopic relationships among the angrites Lewis Cliff 86010 and Angra dos Reis. *Geochim. Cosmochim. Acta* **56,** 1673-1694.

Lugmair G.W. and Marti K. (1977) Sm-Nd-Pu timepieces in the Angra dos Reis meteorite. *Earth Planet. Sci. Lett.* **35,** 273-284.

Ma M.-S., Murali A.V. and Schmitt R.A. (1977) Genesis of the Angra dos Reis and other achondritic meteorites. *Earth Planet. Sci. Lett.* **35,** 331-346.

McCoy T.J., Keil K., Muenow D.W. and Wilson L. (1997) Partial melting and melt migration in the acapulcoite-lodranite parent body. *Geochim. Cosmochim. Acta* **61,** 639-650.

McKay G., Lindstrom D., Yang S.-R. and Wagstaff J. (1988a) Petrology of a unique achondrite Lewis Cliff 86010 (abstract). *Lunar Planet. Sci.* **XIX,** 762-763.

McKay G., Lindstrom D., Le L. and Yang S.-R. (1988b) Experimental studies of synthetic LEW86010 analogs: Petrogenesis of a unique achondrite (abstract). *Lunar Planet. Sci.* **XIX,** 760-761.

McKay G., Le L. and Wagstaff J. (1991) Olivines in angrite LEW87051: Phenos or xenos? achondrite (abstract). *Meteoritics* **26,** 370.

McKay G., Crozaz G., Mikouchi T. and Miyamoto M. (1995) Exotic olivine in antarctic angrites Lewis Cliff 87051 and Asuka 881371 (abstract). *Meteoritics* **30,** 543-544.

Mikouchi T. and McKay G. (2001) Mineralogical investigation of D'Orbigny: A new angrite showing close affinities to Asuka 881371, Sahara 99555 and Lewis Cliff 87051 (abstract). *Lunar Planet. Sci.* **32,** #1876.

Mikouchi T., Takeda H., Miyamoto M., Ohsumi K. and McKay G.A. (1995) Exsolution lamellae of kirschsteinite in magnesium-iron olivine from an angrite meteorite. *Am. Mineral.* **80,** 585-592.

Mikouchi T., Miyamoto M. and McKay G.A. (1996) Mineralogical study of angrite Asuka-881371: Its possible relation to angrite LEW87051. *Proc. NIPR Sym. Ant. Meteorites* **9,** 174-188.

Mikouchi T., McKay G., Le L. and Mittlefehldt D.W. (2000a) Preliminary examination of Sahara 99555: Mineralogy and experimental studies of a new angrite (abstract). *Lunar Planet. Sci.* **31,** #1970.

Mikouchi T., McKay G. and Le L. (2000b) A new angrite Sahara 99555: Mineralogical comparison with Angra dos Reis, Lewis Cliff 86010, Lewis Cliff 87051, ad Asuka 881371 angrites (abstract). *Ant. Meteorites* **25,** 74-76.

Mittlefehldt D.W. (1994) The genesis of diogenites and HED parent body petrogenesis. *Geochim. Cosmochim. Acta* **58,** 1537-1552.

Mittlefehldt D.W. and Lindstrom M.M. (1990) Geochemistry and genesis of the angrites. *Geochim. Cosmochim. Acta* **54,** 3209-3218.

Mittlefehldt D.W., McCoy T.J., Goodrich C.A. and Kracher A. (1998) Non-chondritic meteorites from asteroidal bodies. In *Planetary Materials* (ed. J.J. Papike), pp. 4-1 to 4-195. Reviews in Mineralogy, **36,** Min. Soc. Am., Washington, D.C., USA.

Mittlefehldt D.W., Killgore M. and Lee M.T. (2001) Petrology and geochemistry of the new angrite D'Orbigny (abstract). *Lunar Planet. Sci.* **32,** #2057.

Nyquist L.E. , Bansal B., Wiesmann H. and Shih C.-Y. (1994) Neodymium, strontium and chromium isotopic studies of the LEW86010 angrite and Angra dos Reis meteorites and the chronology of the angrite parent body. *Meteoritics* **29,** 872-885.

Premo W.R. and Tatsumoto M. (1995) Pb isotopic systematics of angrite Asuka-881371 (abstract). *Ant. Meteorites* **20,** 204-206.

Prinz M. and Weisberg M.K. (1995) Asuka 881371 and the angrites: Origin in a heterogeneous, CAI-enriched, differentiated, volatile-depleted body (abstract). *Ant. Meteorites* **20,** 207-210.

Prinz M., Keil K., Hlava P.F., Berkley J.L., Gomes C.B. and Curvello W.S. (1977) Studies of Brazilian meteorites, III. Origin and history of the Angra dos Reis achondrite. *Earth Planet. Sci. Lett.* **35,** 317-330.

Stolper E. (1977) Experimental petrology of eucrite meteorites. *Geochim. Cosmochim. Acta* **41,** 587-611.Takeda H. and Graham A.L. (1991) Degree of equilibration of eucritic pyroxenes and thermal metamorphism of the earliest planetary crust. *Meteoritics* **26,** 129-134.

Takeda H., Bogard D.D., Mittlefehldt D.W. and Garrison D.H. (2000) Mineralogy, petrology, chemistry, and ^{39}Ar-^{40}Ar and exposure ages of the Caddo County IAB iron: Evidence for early partial melt segregation of a gabbro area rich in plagioclase-diopside. *Geochim. Cosmochim. Acta* **64,** 1311-1327.

Tera F., Eugster O., Burnett D.S. and Wasserburg G.J. (1970) Comparative study of Li, Na, K, Rb, Cs, Ca, Sr and Ba abundances in achondrites and in Apollo 11 lunar samples. *Proc. Apollo 11 Lunar Sci. Conf.* 1637-1657.

Varela M.E., Kurat G., Brandstätter F., Bonnin-Masbah M. and Metrich N. (2001) Glasses in the D'Orbigny angrite (abstract). *Lunar Planet. Sci.* **32,** #1803.

Warren P.H. and Davis A.M. (1995) Consortium investigation of the Asuka-881371 angrite: Petrographic, electron microprobe, and ion microprobe observations (abstract). *Ant. Meteorites* **20,** 257-260.

Warren P.H., Kallemeyn G.W. and Mayeda T. (1995) Consortium investigation of the Asuka-881371 angrite: Bulk-rock geochemistry and oxygen isotopes (abstract). *Ant. Meteorites* **20,** 261-264.

Wasserburg G.J., Tera F., Papanastassiou D.A. and Huneke J.C. (1977) Isotopic and chemical investigations on Angra dos Reis. *Earth Planet. Sci. Lett.* **35,** 294-316.

Weigel A., Eugster O., Koeberl C. and Krähenbühl U. (1997) Differentiated achondrites Asuka 881371, an angrite, and Divnoe: Noble gases, ages, chemical composition, and relation to other meteorites. *Geochim. Cosmochim. Acta* **61,** 239-248.

Wilson L. and Keil K. (1997) The fate of pyroclasts produced in explosive eruptions on the asteroid 4 Vesta. *Meteoritics Planet. Sci.* **32,** 813-823.

Wood J.A. and Pellas P. (1991) What heated the meteorite planets? In *The Sun in Time* (eds. C.P. Sonnett, M.S. Giampapa and M.S. Matthews), pp. 740-760. Univ. Arizona Press, Tucson, AZ, USA.

Yanai K. (1994) Angrite Asuka-881371: Preliminary examination of a unique meteorite in the Japanese collection of Antarctic meteorites. *Proc. NIPR Sym. Ant. Meteorites* **7,** 30-41.

Table 1. Representative average olivine and subcalcic kirschsteinite compositions and standard deviations for D'Orbigny.

	olivine												subcalcic kirschsteinite							
	ave	std	ave	std	ave	std	ave	std	ave	std	ave	std	ave	std	ave	std	ave	std	ave	std
n*	6		5		7		6		6		4		3		3		3		3	
SiO_2	36.3	0.1	32.2	0.3	31.4	0.3	31.3	0.4	30.6	0.1	30.4	0.1	31.7	0.1	31.64	0.04	31.46	0.04	31.0	0.4
TiO_2	0.017	0.005	0.06	0.01	0.074	0.007	0.09	0.01	0.114	0.005	0.109	0.005	0.079	0.003	0.09	0.01	0.090	0.004	0.089	0.006
Al_2O_3	0.070	0.002	0.032	0.007	0.026	0.002	0.030	0.008	0.027	0.003	0.029	0.005	0.014	0.002	0.06	0.04	0.016	0.001	0.015	0.002
Cr_2O_3	0.043	0.006	0.004	0.004	-		-		-		-		-		-		-		-	
FeO	30.9	0.2	53.8	0.6	56.7	0.5	54.8	0.8	57.9	0.2	59.3	0.4	45.7	0.1	48.0	0.3	47.8	0.1	48.8	0.6
MnO	0.326	0.005	0.71	0.01	0.80	0.02	0.809	0.008	0.802	0.007	0.73	0.04	0.679	0.005	0.72	0.01	0.70	0.01	0.58	0.03
MgO	31.0	0.2	10.2	0.3	5.3	0.2	3.06	0.09	1.0	0.1	0.09	0.02	1.85	0.05	1.93	0.04	1.17	0.02	0.04	0.02
CaO	0.89	0.01	3.5	0.4	6.0	0.3	10.4	0.5	9.6	0.2	9.2	0.4	20.63	0.07	18.2	0.4	19.3	0.2	19.3	0.2
sum	99.546		100.506		100.301		100.491		100.044		99.859		100.654		100.641		100.537		99.825	
molar Fe/Mn, $100*Mg/(Mg+Fe)$ and mole percent $Ca/(Ca+Mg+Fe)$, etc.																				
Fe/Mn	93.6		74.3		69.6		66.9		71.3		80.8		66.5		66.0		67.4		82.5	
mg#	64.2		25.3		14.4		9.1		3.1		0.3		6.7		6.7		4.2		0.1	
Ca	1.3		5.9		10.5		18.0		17.1		16.6		35.0		31.2		33.2		33.6	
Mg	63.3		23.8		12.9		7.4		2.5		0.2		4.4		4.6		2.8		0.1	
Fe	35.4		70.3		76.7		74.5		80.4		83.2		60.6		64.2		64.0		66.3	
atoms per formula unit based on 4 oxygens																				
Si	0.99413		0.99866		1.00145		1.00196		1.00087		1.00342		0.99605		0.99929		0.99765		0.99725	
Ti	0.00035		0.00128		0.00177		0.00226		0.00280		0.00270		0.00187		0.00221		0.00215		0.00216	
Al	0.00221		0.00115		0.00096		0.00111		0.00102		0.00111		0.00051		0.00205		0.00059		0.00056	
Cr	0.00093		0.00010		-		-		-		-		-		-		-		-	
Fe	0.70710		1.39227		1.51098		1.46681		1.58329		1.63532		1.20310		1.26696		1.26840		1.31525	
Mn	0.00756		0.01873		0.02172		0.02192		0.02220		0.02024		0.01810		0.01919		0.01883		0.01594	
Mg	1.26546		0.47107		0.25332		0.14610		0.04983		0.00423		0.08665		0.09092		0.05521		0.00183	
Ca	0.02621		0.11619		0.20607		0.35500		0.33578		0.32628		0.69548		0.61684		0.65704		0.66730	

* Number of analyses averaged.

Table 2. Representative average clinopyroxene compositions and standard deviations for D'Orbigny.

	ave	std	ave	std	ave	std	ave	std	ave	std	ave	std	ave	std	ave	std
n*	7		7		6		4		4		3		10		7	
SiO_2	45.9	0.1	46.4	0.3	44.8	0.6	43.0	0.2	45.9	0.2	41.1	0.4	40.5	0.2	41.3	0.4
TiO_2	1.47	0.04	1.33	0.08	1.80	0.07	2.4	0.1	1.48	0.04	3.0	0.2	3.2	0.1	3.1	0.4
Al_2O_3	9.0	0.1	7.5	0.3	8.0	0.4	8.8	0.3	4.55	0.04	9.1	0.1	7.7	0.3	5.8	0.9
Cr_2O_3	0.54	0.07	0.27	0.04	0.015	0.006	-		-		-		-		-	
FeO	11.7	0.1	12.67	0.08	16.7	0.3	20.2	0.2	22.7	0.4	22.9	0.5	26.0	0.1	27.3	0.2
MnO	0.133	0.002	0.148	0.008	0.173	0.008	0.188	0.006	0.237	0.002	0.19	0.01	0.174	0.006	0.20	0.006
MgO	9.01	0.06	9.0	0.1	5.9	0.1	3.3	0.1	3.2	0.2	1.34	0.02	0.006	0.008	-	0.008
CaO	23.51	0.05	23.1	0.2	23.3	0.3	23.20	0.09	22.95	0.07	22.7	0.3	22.4	0.1	22.15	0.08
sum	101.263		100.418		100.688		101.089		101.017		100.333		99.980		99.850	
					molar Fe/Mn, 100*Mg/(Mg+Fe) and mole percent Ca/(Ca+Mg+Fe), etc.											
Fe/Mn	86.5		84.5		95.2		106.0		94.6		119.7		147.6		135.9	
mg#	57.9		55.7		38.6		22.5		19.9		9.5		0.0		0.0	
Ca	52.1		50.9		52.3		53.3		50.9		53.5		52.5		51.0	
Mg	27.8		27.4		18.4		10.5		9.7		4.4		0.0		0.0	
Fe	20.2		21.7		29.3		36.2		39.3		42.1		47.5		49.0	
					atoms per formula unit based on 6 oxygens											
Si	1.73506		1.77345		1.74664		1.70062		1.83017		1.66396		1.67444		1.71913	
Ti	0.04185		0.03813		0.05275		0.07285		0.04434		0.09131		0.09949		0.09787	
Al	0.39227		0.33120		0.35875		0.40126		0.21010		0.42628		0.36946		0.28076	
Cr	0.01618		0.00807		0.00046		-		-		-		-		-	
Fe	0.36866		0.40516		0.54345		0.66778		0.75843		0.77658		0.89860		0.94956	
Mn	0.00426		0.00479		0.00571		0.00630		0.00801		0.00649		0.00609		0.00699	
Mg	0.50786		0.51030		0.34208		0.19336		0.18785		0.08111		0.00037		-	
Ca	0.95273		0.94767		0.97117		0.98370		0.98154		0.98571		0.99290		0.98830	

* Number of analyses averaged.

30

Table 3. Representative analyses, and representative average spinel compositions and standard deviations for D'Orbigny.

grain	sp01 core		sp01 rim	sp12 core		sp12 rim	sp15		sp07				sp06		sp03		sp04	
	ave	std	ave	ave	std	1	ave	std	1	1	1	1	ave	std	ave	std	ave	std
n*	13		2	4		1	8		1	1	1	1	5		7		3	
TiO_2	0.263	0.006	1.85	0.327	0.005	0.360	0.342	0.004	0.341	0.353	0.358	1.18	27.0	0.1	26.42	0.08	24.79	0.04
SiO_2	0.107	0.008	0.13	0.12	0.02	0.110	0.132	0.007	0.110	0.114	0.112	0.131	0.093	0.004	0.12	0.01	0.136	0.008
Cr_2O_3	8.35	0.05	11.4	10.8	0.2	8.72	9.68	0.07	10.9	9.82	8.39	7.25	0.002	0.005	0.003	0.003	0.004	0.003
Al_2O_3	54.4	0.1	42.6	51.9	0.1	52.2	52.0	0.1	51.3	51.8	52.8	47.2	2.08	0.07	2.88	0.02	3.35	0.07
V_2O_3	0.168	0.003	0.31	0.189	0.001	0.203	0.203	0.003	0.194	0.199	0.203	0.142	-		-		-	
Fe_2O_3	2.3	0.1	6.24	2.2	0.1	2.60	2.44	0.06	2.64	2.70	2.49	5.06	12.3	0.2	12.3	0.2	14.9	0.1
FeO	19.85	0.04	29.6	20.6	0.1	22.8	21.83	0.08	20.9	21.5	22.5	31.4	55.3	0.2	54.9	0.1	53.52	0.02
MnO	0.129	0.005	0.20	0.129	0.007	0.143	0.137	0.004	0.135	0.146	0.142	0.250	0.292	0.009	0.224	0.007	0.23	0.01
MgO	13.55	0.04	6.78	12.82	0.06	11.2	11.84	0.03	12.6	12.1	11.5	5.32	0.072	0.009	0.011	0.004	0.004	0.002
CaO	0.004	0.006	0.10	0.053	0.005	0.141	0.20	0.02	0.070	0.109	0.200	0.218	0.05	0.01	0.13	0.03	0.17	0.03
sum	99.121		99.234	99.138		98.477	98.804		99.190	98.841	98.695	98.151	97.189		96.988		97.104	
Fe/Mn	152		146	158		157	157		153	146	156	124	187		242		229	
molar Fe/Mn and mole percent mineral end members, chromite, etc.																		
cm	9.06		13.54	11.93		9.73	10.73		12.05	10.87	9.30	8.57	0.00		0.00		0.01	
hc	32.57		44.91	31.92		39.65	36.45		32.16	35.07	39.35	59.40	4.28		6.42		7.51	
sp	55.43		30.33	53.19		47.09	49.53		52.30	50.47	47.96	23.68	77.59		75.89		71.07	
uv	0.54		4.18	0.68		0.76	0.72		0.72	0.74	0.76	2.65	0.41		0.06		0.02	
mt	2.39		7.04	2.28		2.76	2.57		2.77	2.85	2.63	5.69	17.71		17.62		21.39	
atoms per formula unit based on 4 oxygens																		
Ti	0.00540		0.04152	0.00681		0.00760	0.00717		0.00712	0.00739	0.00752	0.02640	0.77315		0.75550		0.70703	
Si	0.00292		0.00375	0.00343		0.00309	0.00368		0.00306	0.00318	0.00313	0.00389	0.00354		0.00453		0.00516	
Cr	0.18030		0.26872	0.23721		0.19353	0.21337		0.23966	0.21619	0.18505	0.17048	0.00006		0.00009		0.00012	
Al	1.75170		1.49359	1.69269		1.72556	1.70923		1.68047	1.70159	1.73679	1.65236	0.09355		0.12914		0.14993	
V	0.00368		0.00731	0.00420		0.00457	0.00454		0.00432	0.00444	0.00454	0.00338						
Fe^{3+}	0.04767		0.13985	0.04543		0.05497	0.05115		0.05520	0.05664	0.05234	0.11318	0.35301		0.35071		0.42559	
Fe^{2+}	0.45352		0.73608	0.47671		0.53467	0.50929		0.48462	0.50194	0.52425	0.78158	1.76096		1.74691		1.69765	
Mn	0.00299		0.00504	0.00303		0.00340	0.00324		0.00318	0.00345	0.00336	0.00629	0.00629		0.00722		0.00742	
Mg	0.55170		0.30101	0.52891		0.46838	0.49230		0.52029	0.52194	0.47705	0.23549	0.00409		0.00062		0.00023	
Ca	0.00012		0.00313	0.00157		0.00424	0.00604		0.00208	0.00325	0.00598	0.00694	0.00220		0.00530		0.00687	

* Number of analyses averaged.

Sp01 – large, rounded spinel grain; sp07, sp12, sp15 – small, euhedral hercynitic spinels; sp03, sp04, sp06 – mesostasis ulvöspinels.

Table 4. Representative average compositions of plagioclase, silico-phosphate, and unknown Fe-Ca-Al-Ti-silicate.

	plag	silico-phosphate				Fe-Ca-Al-Ti-silicate		
n[*]	4	4	6	8	2	10	12	9
SiO_2	43.6	12.2	13.4	13.8	19.0	25.6	25.6	25.4
TiO_2	-	1.42	1.64	1.61	1.61	8.77	9.39	9.25
Al_2O_3	36.2	0.27	0.41	0.45	2.11	10.5	10.3	10.5
Cr_2O_3	-	0.0	0.0	0.0	0.0	0.0	0.0	0.0
FeO	0.65	4.99	5.45	5.94	9.51	41.2	41.0	41.1
MnO	-	0.07	0.07	0.08	0.08	0.17	0.17	0.18
MgO	0.15	0.0	0.01	0.0	0.0	0.0	0.04	0.02
CaO	20.0	48.7	50.9	47.3	41.9	12.5	12.5	12.6
Na_2O	0.02	-	-	-	-	-	-	-
K_2O	0.0	-	-	-	-	-	-	-
P_2O_5	-	29.7	24.5	28.1	21.9	0.08	0.08	0.07
sum	100.62	97.35	96.38	97.28	96.11	98.82	99.08	99.12

[*] Number of analyses averaged.

Table 5. Major element composition and CIPW normative mineralogy of D'Orbigny compared to literature data for angrites.[*]

	D'Orbigny wr	D'Orbigny glass	Angra dos Reis	LEW 86010	LEW 87051	Asuka 881371
SiO_2	38.3	39.3	43.7	39.6	40.4	37.3
TiO_2	0.88	0.78	2.05	1.15	0.73	0.88
Al_2O_3	12.4	12.3	9.35	14.1	9.19	10.1
Cr_2O_3	0.0419	0.06	0.219	0.118	0.159	0.139
FeO_T	24.8	24.8	9.4	18.5	19.0	24.0
MnO	0.28	0.27	0.10	0.20	0.24	0.20
MgO	6.56	7.1	10.8	7.0	19.4	14.8
CaO	15.1	15.2	22.9	17.5	10.8	12.5
Na_2O	0.0172	-	0.0301	0.0211	0.0234	0.0216
P_2O_5	0.16	-	0.13	0.13	0.08	0.17
sum	98.54	99.81	98.68	98.32	100.02	100.11
molar Fe/Mn, 100*Mg/(Mg+Fe) and (Ca/Al)$_{CI}$.						
Fe/Mn	87	91	93	91	78	118
mg#	32.0	33.8	67.2	40.3	64.5	52.4
$(Ca/Al)_{CI}$	1.54	1.56	3.09	1.57	1.48	1.56
CIPW norm						
Ol	37.6		13.1	28.2	52.5	55.3
Cs	5.64		9.67	6.80	1.97	8.27
Di	19.2		46.3	22.2	17.7	5.52
An	34.2		25.7	39.0	25.0	27.4
Ne	0.08		0.14	0.10	0.11	0.10
Cm	0.06		0.33	0.18	0.23	0.19
Il	1.69		3.94	2.22	1.38	1.67
Mt	1.22		0.46	0.91	0.92	1.16
Ap	0.38		0.30	0.31	0.19	0.39

* D'Orbigny – whole rock (wr), this work, major elements determined by fused-bead, electron microprobe analysis; Cr_2O_3 and Na_2O by INAA (average of data in Table 6); glass – average of glass patches, sphere, and glass with bubbles, Varela et at. (2001). Angra dos Reis, LEW 86010 and LEW 87051 – Mittlefehldt and Lindstrom (1990), major elements determined by fused-bead, electron microprobe analysis; Cr_2O_3 and Na_2O by INAA. A-881371 – Yanai (1994), major elements by wet chemistry; Warren *et al.* (1995) Cr_2O_3 and Na_2O by INAA. CIPW norm calculated assuming molar Fe^{3+}/Fe^{2+} of 0.03.

Page intentionally left blank

Table 6. Select major, minor and trace element contents of angrites D'Orbigny and Sahara 99555, and USGS standard rock BHVO-1.[*]

| | | D'Orbigny | | | | | | Sahara 99555 | | | BHVO-1^{+} | |
											JSC	lit.
mass (mg)[†]		55.88			53.34			28.89				
Na$_2$O	wt%	0.01962	±	0.00026	0.01473	±	0.00020	0.01639	±	0.00025	2.300	2.26
K	µg/g	137[‡]	±	10	69	±	15	44	±	19	4230	4320
CaO	wt%	17.8	±	1.6	15.0	±	0.5	15.1	±	0.5	11.0	11.4
Sc	µg/g	46.3	±	0.5	40.3	±	0.4	50.7	±	0.6	31.3	31.8
Cr	µg/g	311	±	3	262	±	3	317	±	3	292	289
FeO	wt%	24.93	±	0.27	25.40	±	0.28	23.73	±	0.26	10.9	11.0
Co	µg/g	34.7	±	0.4	33.0	±	0.4	31.2	±	0.4	45.0	45
Ni	µg/g	56	±	15	91	±	15	<80			120	121
As	µg/g	0.52	±	0.04	0.53	±	0.05	1.98	±	0.10	0.54	0.4[+]
Se	µg/g	0.53	±	0.21	0.74	±	0.21	1.2	±	0.3	nd	
Sr	µg/g	126	±	21	142	±	24	107	±	21	390	403
Zr	µg/g	70	±	18	66	±	19	nd			160	179
Sb	µg/g	0.057	±	0.018	<0.034			<0.05			0.16	0.16
Ba	µg/g	47	±	18	52	±	7	45	±	17	125	139
La	µg/g	3.56	±	0.04	3.76	±	0.04	3.20	±	0.04	15.22	15.8
Ce	µg/g	8.78	±	0.26	9.18	±	0.24	8.41	±	0.24	37.8	39
Nd	µg/g	nd			5.4	±	2.6	nd			28	25.2
Sm	µg/g	2.161	±	0.029	2.23	±	0.03	2.107	±	0.028	6.05	6.2
Eu	µg/g	0.846	±	0.016	0.876	±	0.017	0.829	±	0.018	2.06	2.06
Tb	µg/g	0.534	±	0.019	0.511	±	0.018	0.512	±	0.023	0.95	0.96
Yb	µg/g	2.12	±	0.06	2.13	±	0.04	2.12	±	0.04	1.98	2.02
Lu	µg/g	0.309	±	0.013	0.308	±	0.007	0.319	±	0.009	0.274	0.291
Hf	µg/g	1.63	±	0.06	1.48	±	0.05	1.80	±	0.06	4.61	4.38
Ta	ng/g	192	±	13	200	±	14	192	±	16	1.13	1.23
W	ng/g	180	±	60	nd			360	±	90	nd	
Ir	ng/g	nd			<2			<4			nd	
Au	ng/g	69.7[§]	±	2.5	<2			<3			nd	
Th	ng/g	370	±	40	434	±	29	360	±	40	1.12	1.08
U	ng/g	<210			116	±	22	<210			0.33	0.42

[*] Determined by INAA. Uncertainties are ±1σ, upper limits are 2σ, nd is not determined.

[†] Mass of sample analyzed. The first D'Orbigny sample and Sahara 99555 are splits of homogenized powders of larger samples. See text.

[‡] High K value likely represents contamination by fine-grained terrestrial sediment. The second D'Orbigny sample was cleaned in triply-distilled water in an ultrasonic bath before crushing for analysis. See text.

[§] High Au value likely represents contamination during handling.

[+] JSC – average of two analyses, lit. - Govindaraju (1994); As is an information only value.
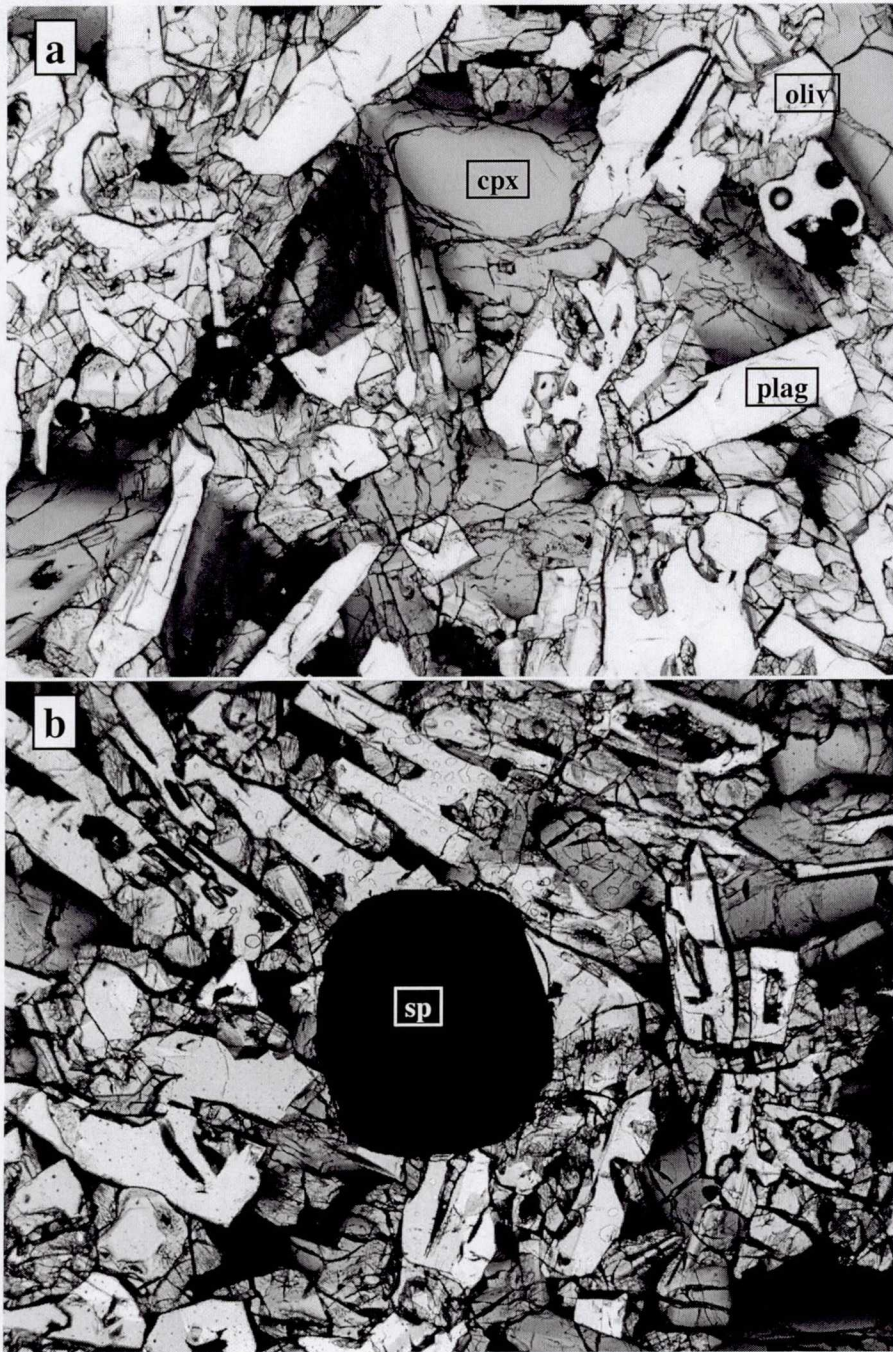
Figure 1. Photomicrographs of general textural features of D'Orbigny. An olivine-plagioclase graphic intergrowth is just below label a. Opaque areas are mesostasis, except for the large, rounded spinel in b. A vesicle occurs below the labeled olivine. Plane-polarized light; fields of view 2.3x1.7 mm.
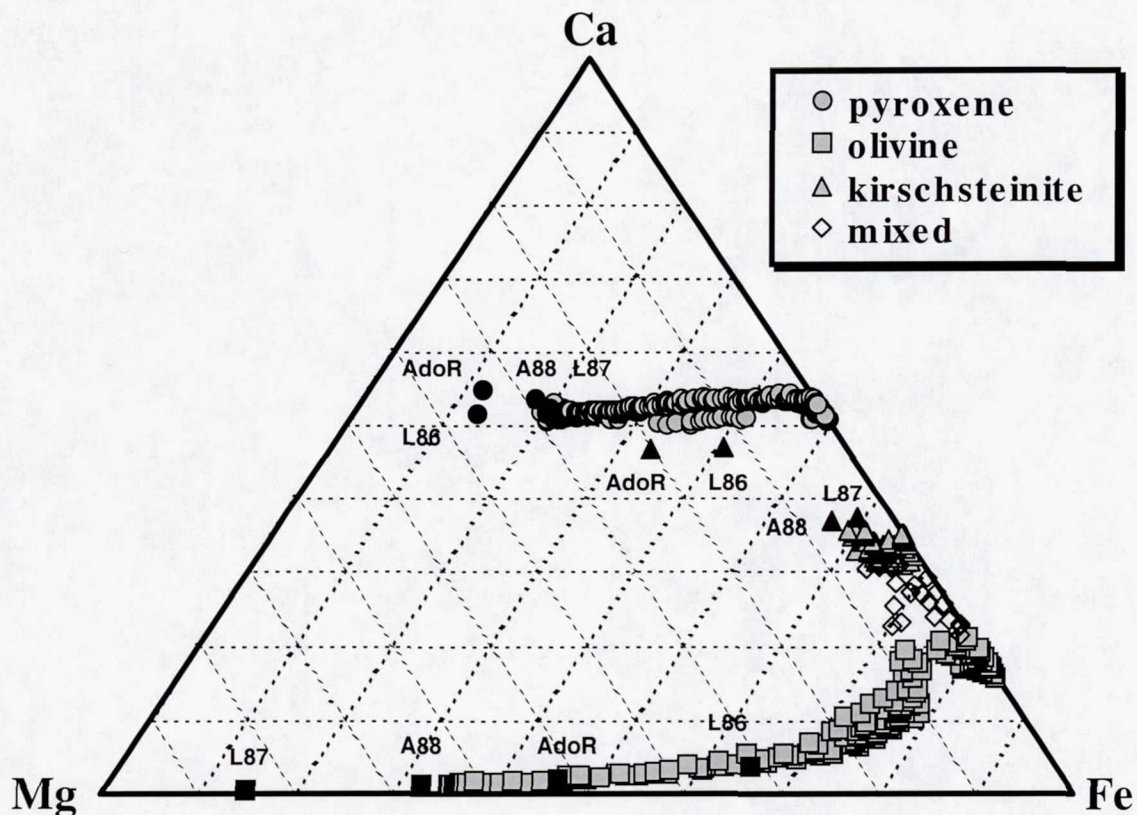
Figure 2. Molar Ca-Mg-Fe triangular diagram of mafic silicates of D'Orbigny compared to literature data for most magnesian compositions for Asuka 881371 (A88), Angra dos Reis (AdoR), Lewis Cliff 86010 (L86) and LEW 87051 (L87). For A-881371 and LEW 87051, olivine phenocryst data are shown. Open symbols (mixed) indicate analyses we believe overlapped both olivine and subcalcic kirschsteinite. Literature data are from Crozaz and McKay (1990), McKay, unpublished, Mikouchi *et al.* (1995, 1996), Prinz *et al.* (1977), Warren and Davis (1995), Yanai (1994).
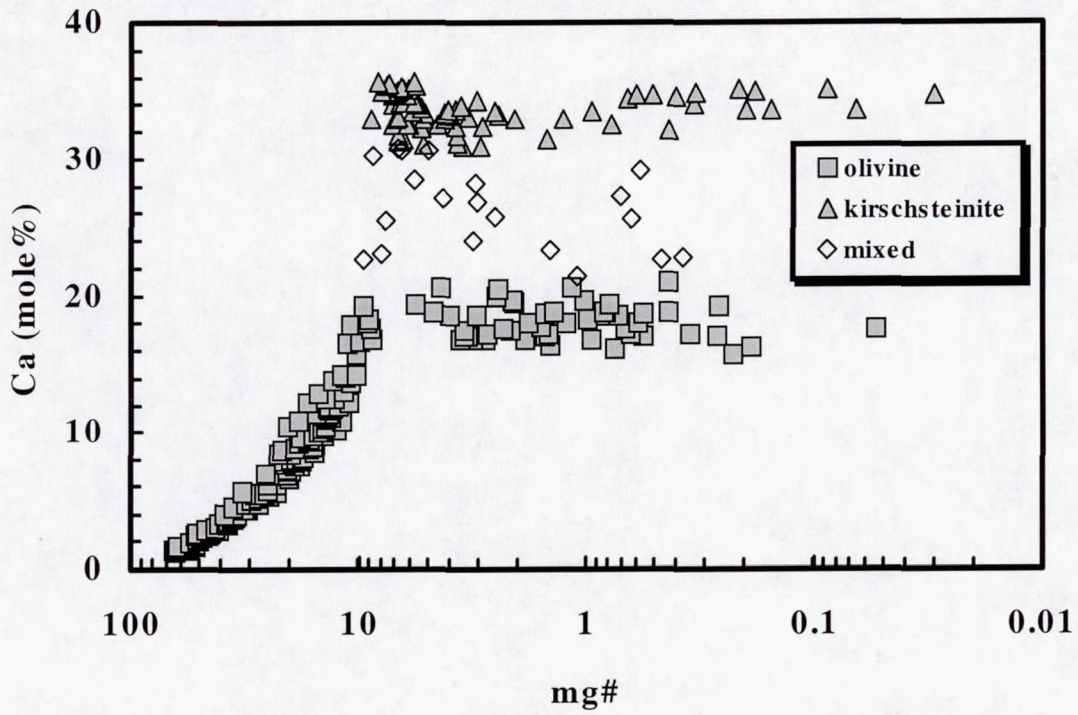
Figure 3. Ca (mole%) *vs.* mg# for olivine and subcalcic kirschsteinite in D'Orbigny. Open symbols (mixed) indicate analyses we believe overlapped both phases. Note distinct gap in olivine compositions between about mg# 9 and 6.
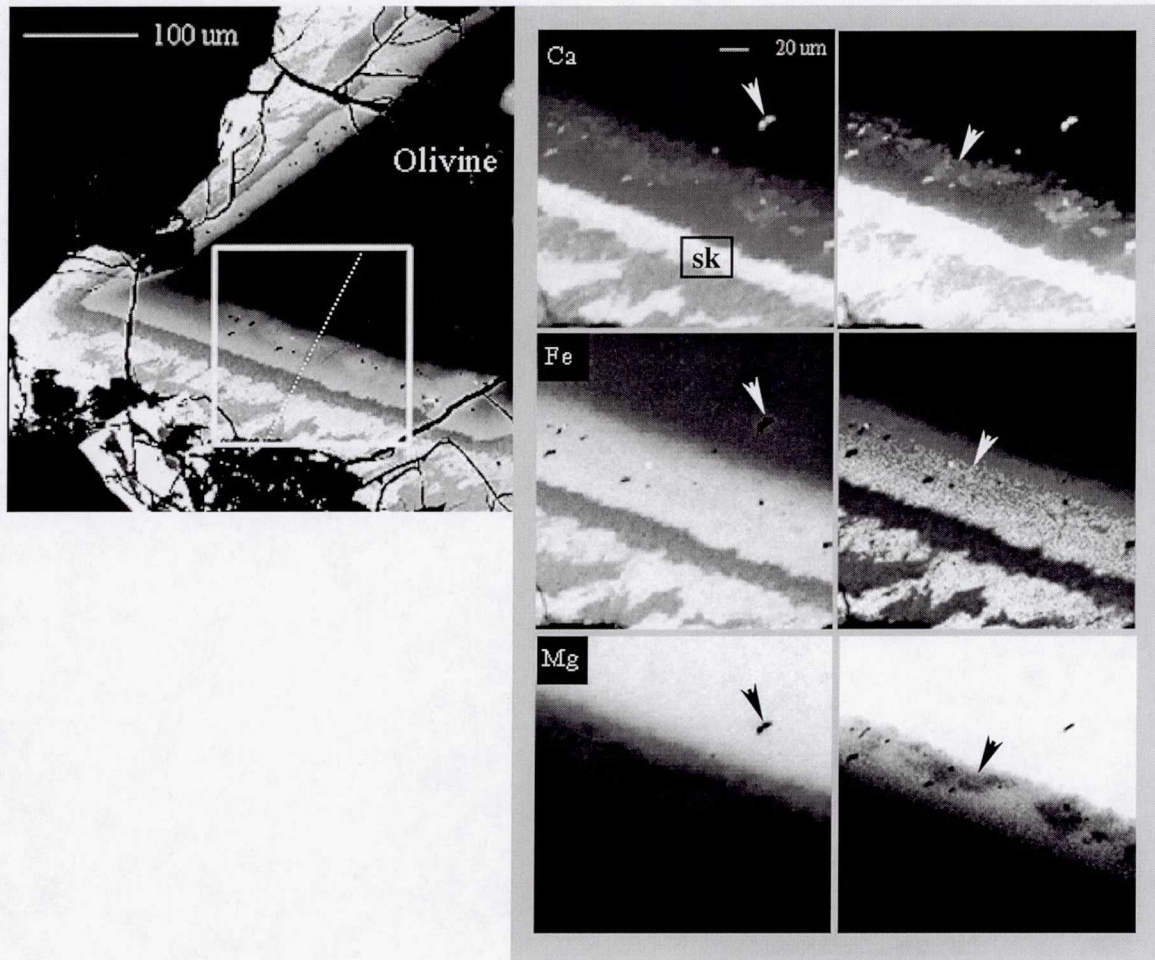
Figure 4. Back-scattered electron image and Ca, Fe and Mg x-ray maps of rim zoning in a composite olivine-subcalcic kirschsteinite grain. The dotted line shows the location of the zoning profile given in Fig. 5. The x-ray maps in the right column have been enhanced to bring out subtle details of the region between the homogeneous Mg-rich core and the first subcalcic kirschsteinite (sk) band. Arrows in right column show remnant Ca- and Fe-rich olivine enveloped by more Mg-rich overgrowths (reverse zoning in Fig. 5). Arrows in left column highlight small, Ca-rich, Fe- and Mg-free inclusions (Ca-phosphate?).
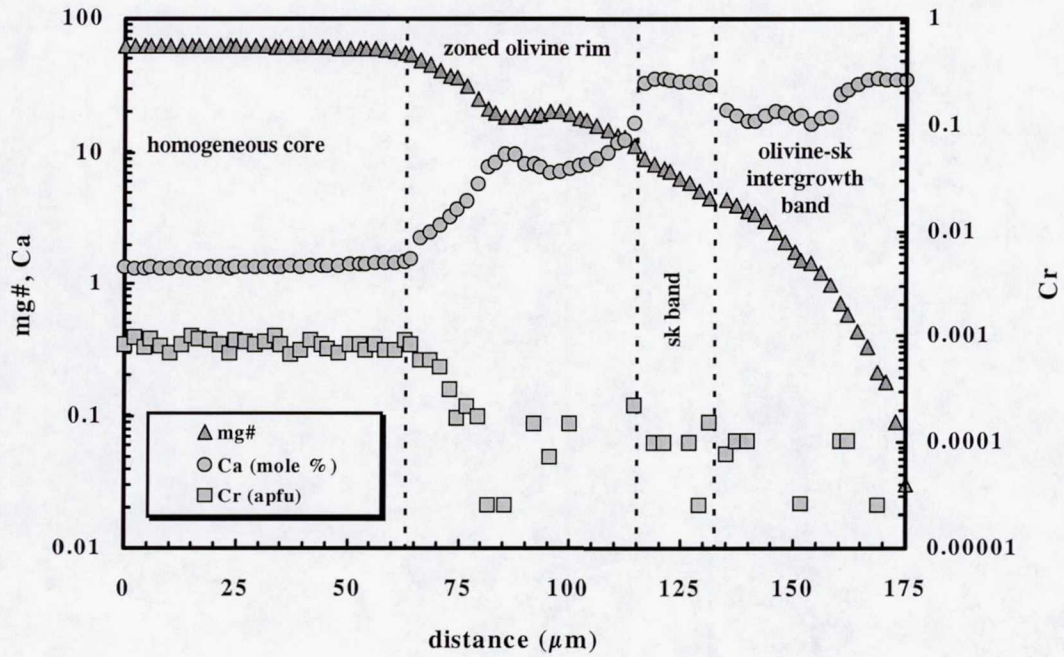
Figure 5. Zoning profile for olivine-subcalcic kirschsteinite grain shown in Fig. 4. Vertical lines break-up the sequence into distinct regions. Note slight zoning reversal in the zoned olivine rim region at ~90-100 μm. Sk = subcalcic kirschsteinite.
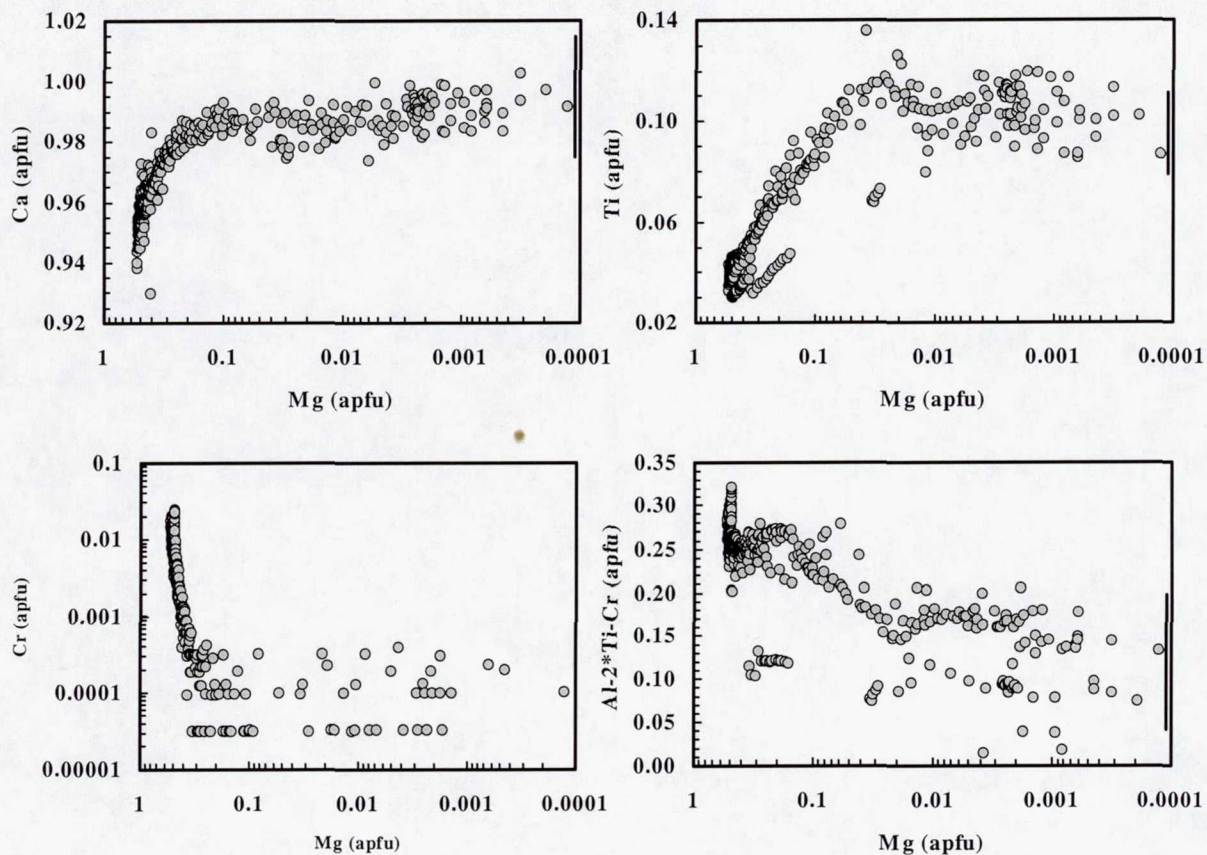
Figure 6. Variation of Ca, Ti, Cr and Al-2*Ti-Cr, Ti with Mg (all in atoms per formula unit) for clinopyroxene. Vertical bars show ranges in compositions for analyses with Mg of 0 apfu. The wide range in Ca at Mg ~0 is due to P-rich clinopyroxene in rim areas intergrown with silico-phosphate. Note that some analyses are distinct in both Ti and Al-2*Ti-Cr.
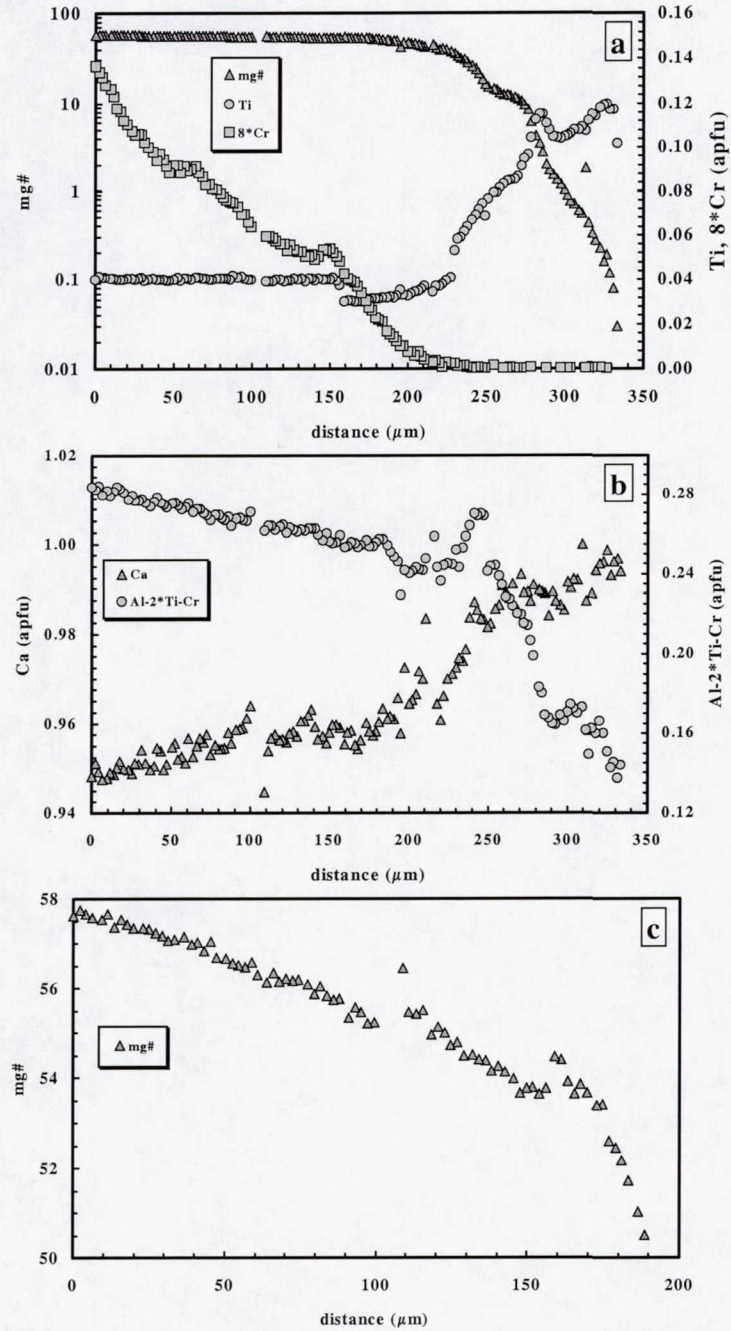
Figure 7. Detailed zoning profile from center to rim of a large clinopyroxene grain in D'Orbigny. Note in particular slight reversals in trends for mg# (expanded in c), and Cr (a), breaks in Ti (a), and variations in Al-2*Ti-Cr (b). Part c shows an expanded view of mg# variations in the central region of the grain.
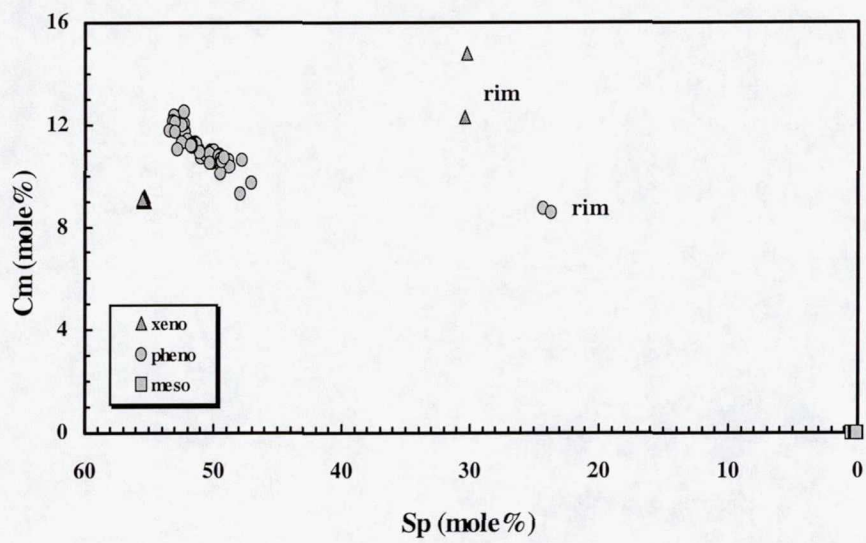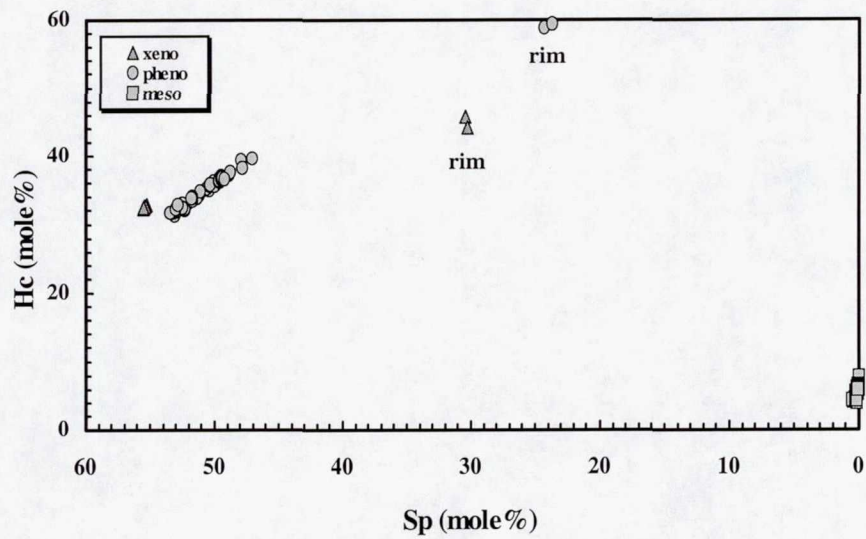
Figure 8. Compositional end-members hercynite and chromite *vs.* spinel of texturally distinct spinel grains; a homogeneous large xenocryst; small zoned euhedral phenocryst grains, and mesostasis grains.
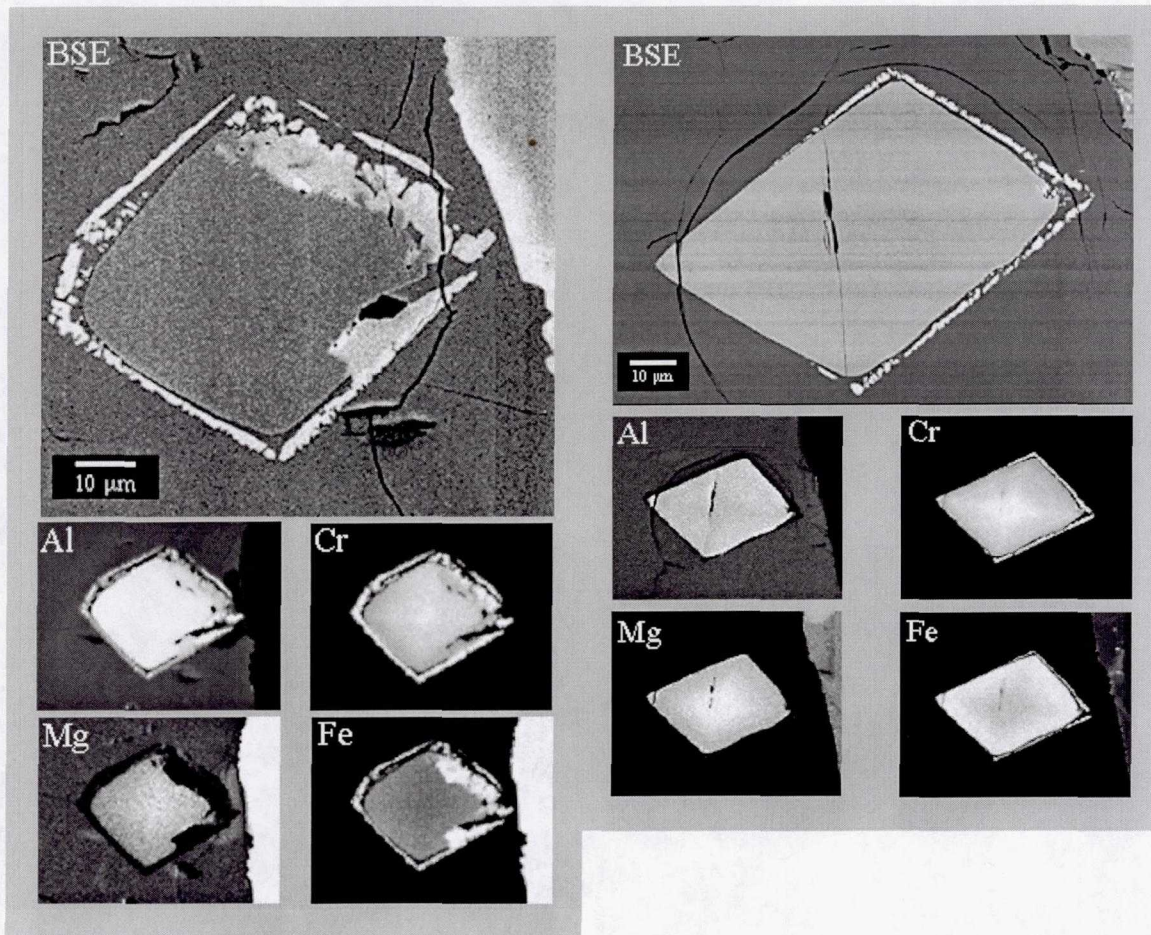
Figure 9. Back-scattered electron images and element maps of euhedral hercynitic spinel grains enclosed in clinopyroxene (left) and plagioclase (right). Note elemental zoning over a scale of a few μm, and Cr-rich rims.
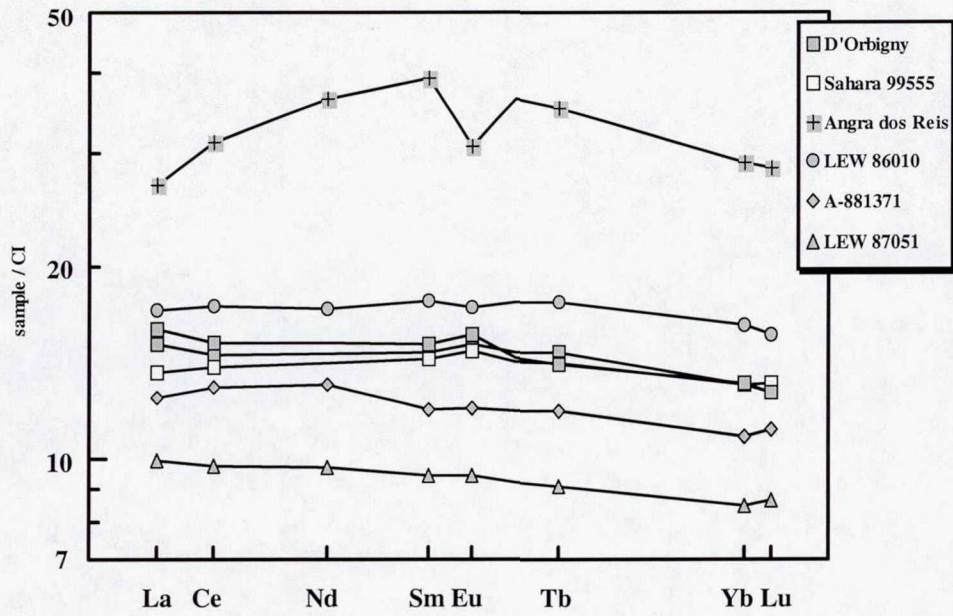
Figure 10. Rare earth element diagram for angrites. D'Orbigny and Sahara 99555 – this work; other angrites – Lugmair and Galer (1992), Ma *et al.* (1977), Mittlefehldt and Lindstrom (1990), Nyquist *et al.* (1994) and Warren *et al.* (1995).
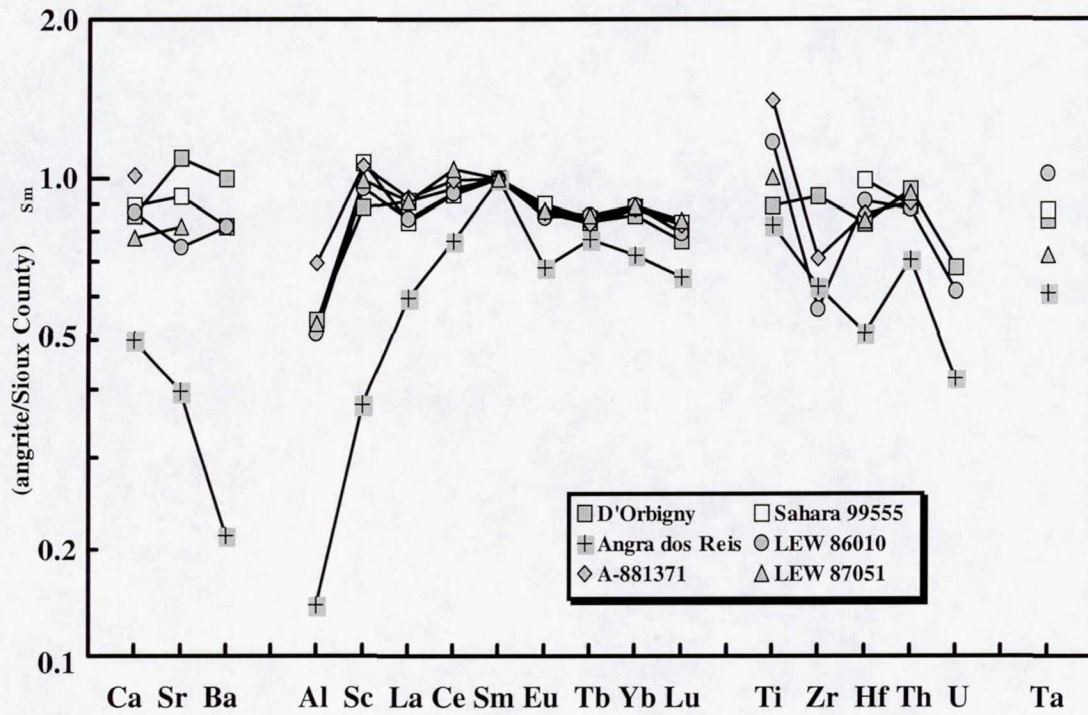
Figure 11. Sioux County- and Sm-normalized incompatible element contents of angrites plotted in order of increasing valence and Z. Data are from the sources listed in Fig. 10, plus Tera *et al.* (1970), Wasserburg *et al.* (1977) and Yanai (1994). Sioux County average calculated from a database of all available literature data.
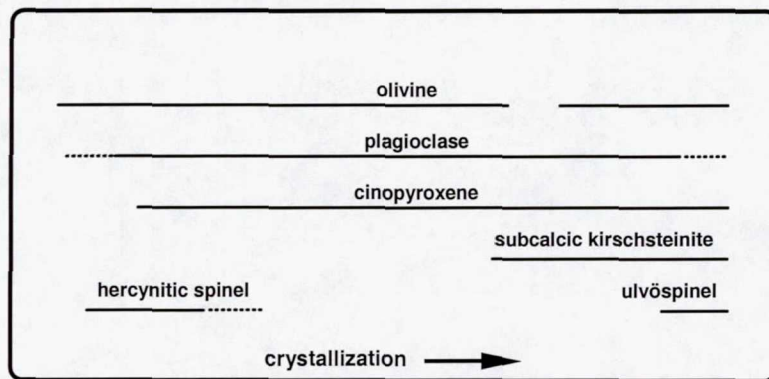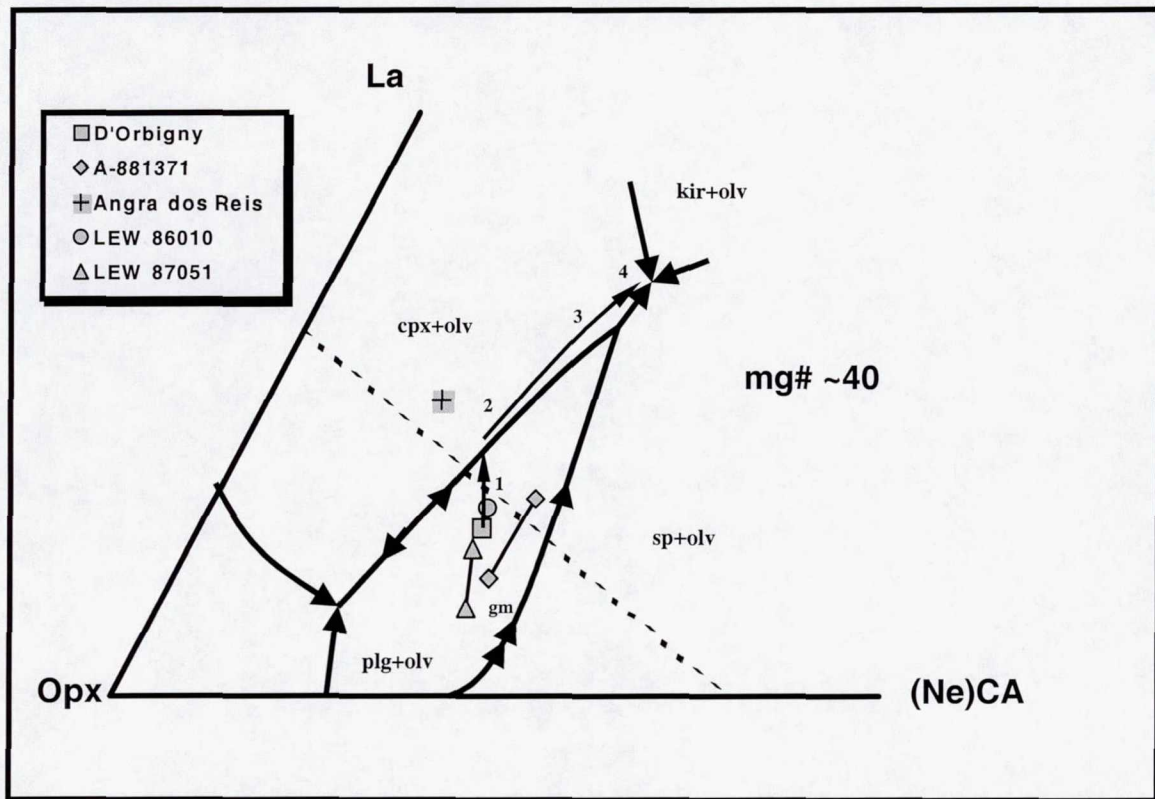
Figure 12. Schematic phase diagram (after Longhi, 1999) and crystallization sequence for D'Orbigny. A-881371 and LEW 87051 are plotted for both their bulk rock (Mittlefehldt and Lindstrom, 1990; Yanai, 1994) and groundmass (gm – Prinz and Weisberg, 1995) compositions. Schematic crystallization path (1-4) is described in the text.
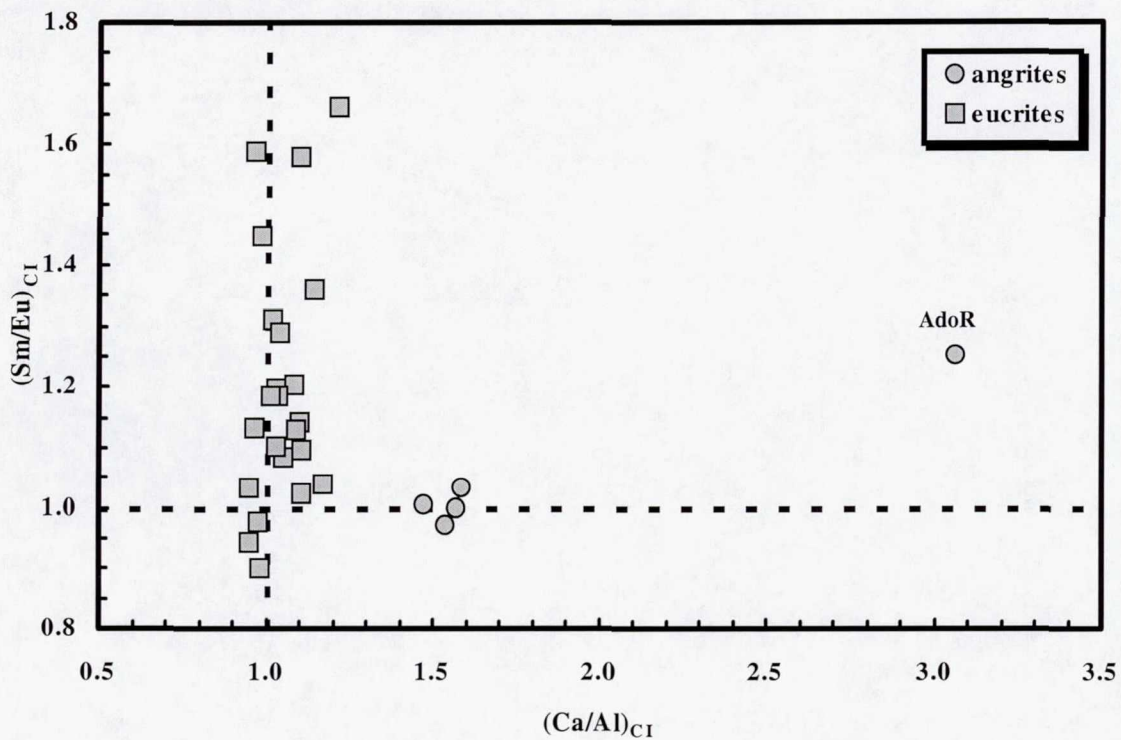
Figure 13. $(Sm/Eu)_{CI}$ *vs.* $(Ca/Al)_{CI}$ for angrites compared to basaltic eucrites. Angrite data are from the sources listed in Figs. 10 and 11. Eucrites show the effect of calcic plagioclase fraction, which increases Sm/Eu but not Ca/Al. Angrites, excluding Angra dos Reis (labeled), show no evidence for plagioclase fractionation, but have fractionated Ca/Al. Eucrite data are averages of all available literature data from a database maintained by the senior author.
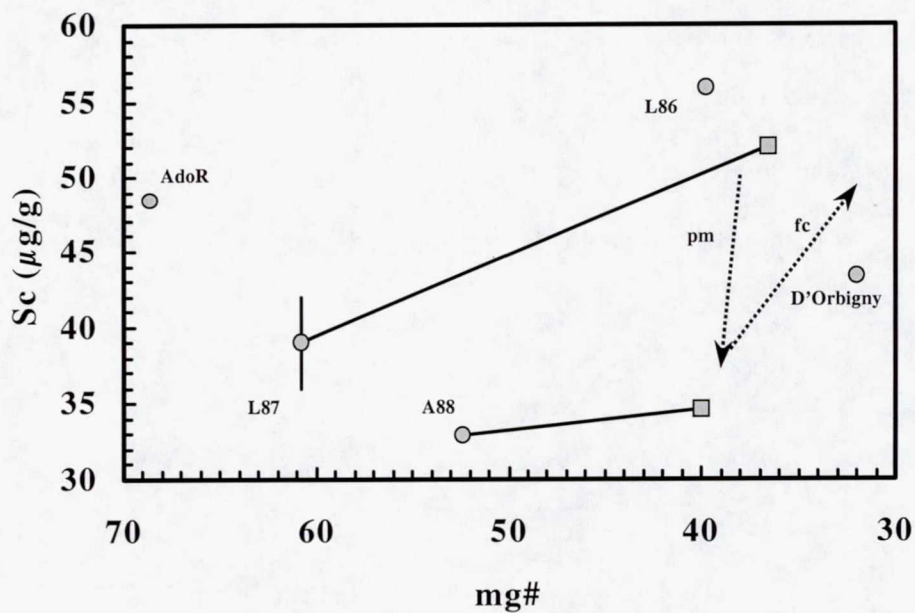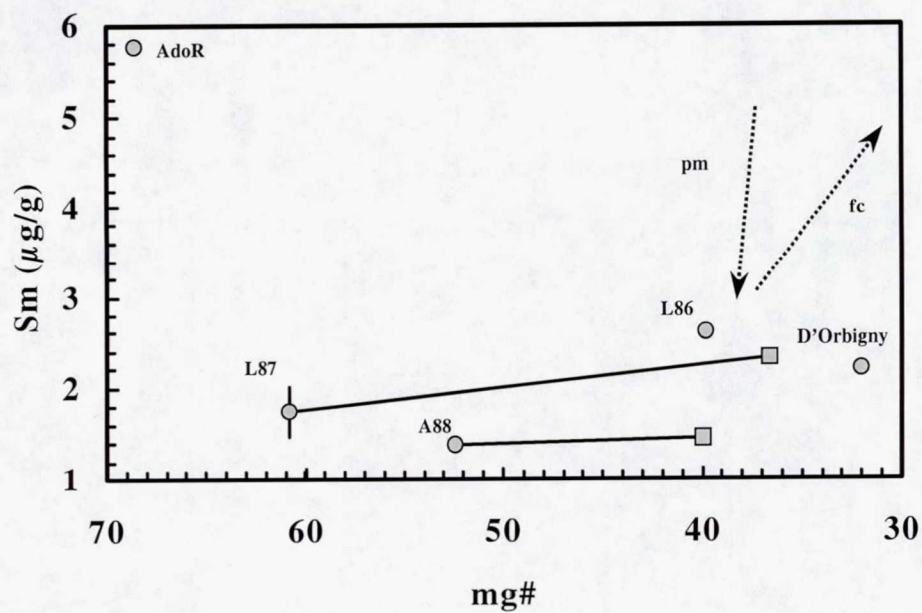
Figure 14. Samarium and Sc *vs.* mg# for D'Orbigny compared to other angrites. For A-881371 and LEW 87051, the bulk (circle) and groundmass (square) compositions are shown. The vertical bar for L87 shows the range of the two available Sm and Sc concentrations. Sources for literature data are given in Figs. 10 and 11, except groundmass mg# calculated from Prinz and Weisberg (1995). Dashed arrows show schematic partial melting and fractional crystallization trends; see text.